Engineering Structures 343 (2025) 121122

Contents lists available at ScienceDirect

Engineering Structures

journal homepage: www.elsevier.com/locate/engstruct

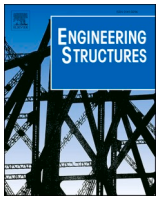

Flexural behaviour, cracking, and serviceability of sustainable RC beams with waste glass fine aggregate and pond ash

V. Fernando [a,*], R. Bastola [a], W. Lokuge [a], C. Gunasekara [b], H. Wang [a]

[a] School of Engineering, Centre for Future Materials, University of Southern Queensland, Springfield, QLD 4300, Australia
[b] Civil and Infrastructure Engineering, School of Engineering, RMIT University, 124 La Trobe Street, Melbourne, VIC 3000, Australia

ARTICLE INFO

Keywords:
Mechanical properties
Glass aggregate
Fly ash
Pond ash
RC beams

ABSTRACT

This study investigates the flexural behaviour of steel-reinforced concrete beams incorporating waste glass fine aggregate (GFA) and unprocessed waste coal ash, known as pond ash (PA), as sustainable alternatives to conventional materials. Driven by environmental concerns over natural sand extraction and the diminishing availability of fly ash for alkali-silica reaction mitigation, the research explores the combined use of GFA and PA to produce sustainable concrete. Concrete tests, including compressive strength, splitting tensile strength, and flexural strength, were conducted to evaluate the mechanical performance. A series of RC beams were cast with varying replacement levels of conventional fine aggregates by GFA (0 %, 20 %, and 40 %) and with ordinary Portland cement (OPC) partially replaced by 20 % of PA. The beams were tested under three-point bending at 28 days and six months, with digital image correlation employed to capture crack propagation and deformation characteristics. The performance of beams was evaluated regarding crack initiation and propagation, crack width evolution, failure mode, load-deflection response, yield and ultimate loads, stiffness, ductility, and energy absorption capacity. The results showed that while GFA increased cracking at 28 days, it reduced crack widths at six months. The addition of PA significantly decreased crack widths at both ages, enhancing serviceability. Yield and ultimate loads remained within ±10 % of the control for all mixes, indicating minimal structural compromise. These results demonstrate that waste glass and unprocessed pond ash can be successfully used in RC beams without sacrificing flexural performance, offering a practical path toward more sustainable structural concrete.

1. Introduction

Aggregates are fundamental to concrete, comprising about 80–85 % of a typical mix. However, their extensive use leads to the unsustainable consumption of local natural resources [1]. The extraction of natural sand, particularly for fine aggregates, leads to the erosion of river deltas and coastlines [2]. To address this environmental concern, researchers have been exploring alternative sustainable materials for aggregates. One such material is waste glass, which can be crushed and used as fine or coarse aggregate [3,4]. Glass is a vital material in modern society, known for its transparency, durability, and versatility in various applications. However, glass waste, which constitutes around 7 % of global solid waste, poses significant environmental challenges as it takes millions of years to decompose [5,6]. Recycling waste glass addresses this issue, but faces several obstacles. The standard recycling process involves sorting, cleaning, and melting waste glass, which is energy-intensive and costly. Producing high-quality recycled glass is difficult due to impurities and colour variations, making it challenging to meet quality standards [7]. As a result, the global glass recycling rate remains low, prompting interest in alternative uses for waste glass [8]. The use of waste glass eliminates the need for sorting and melting, increasing its recycling rate and conserving landfill space. Additionally, it helps mitigate natural resource depletion and reduces the environmental impact on river systems caused by sand extraction. Hence, using waste glass in concrete has the potential to tackle two significant environmental challenges. However, past studies have recognised two major problems with utilising waste glass in concrete.

Previous research has produced conflicting results on the impact of waste glass on concrete strength. Some studies reported a significant reduction in compressive strength when glass fine aggregates (GFA) are used to replace conventional fine aggregates, while others found minimal or even improved strength. For instance, De Castro and De Brito [9] observed a 14 % reduction in strength with 20 % GFA, whereas Batayneh et al. [10] noted a 40 % strength increase with a similar GFA

* Corresponding author.
E-mail address: Vimukthi.fernando@usq.edu.au (V. Fernando).

https://doi.org/10.1016/j.engstruct.2025.121122
Received 2 May 2025; Received in revised form 17 July 2025; Accepted 5 August 2025
Available online 8 August 2025

replacement. Meanwhile, Taha and Nounu [11] reported no significant effect on concrete strength even with 100 % GFA utilisation. This highlights the highly variable effects of GFA on concrete strength. Moreover, the use of glass in concrete poses the risk of Alkali-Silica Reaction (ASR), where amorphous silica in glass reacts with alkalis in cement, causing expansion and cracking [12,13]. Consequently, past studies have shown higher ASR expansion with glass aggregates [14,15]. For example, Abdallah and Fan [14] reported a 325 % increase in ASR expansion with 20 % GFA compared to the control. Nevertheless, previous research has shown that low lime supplementary cementitious materials (SCM) such as class-F fly ash, ground granulated blast-furnace slag and metakaolin can mitigate ASR [16,17]. Fly ash (FA) has been shown to decrease ASR expansion when used with glass aggregates [18,19]. Our recent LCA findings have shown that replacing natural sand with 60 % GFA (<4.75 mm) can substantially reduce the environmental impact of concrete, such as lowering human carcinogenic toxicity by 13 %, compared to conventional mixes [20]. Moreover, the production cost of GFA is estimated at just AUD 1.95 per tonne, making it a highly economical alternative to natural sand. When 60 % GFA is combined with 10 % FA as partial cement replacement, the reductions become more pronounced, achieving a 16.4 % decrease in embodied energy and an 18 % drop in global warming potential, while maintaining comparable mechanical performance [20]. However, FA is becoming scarce with the closure of coal power plants globally. This necessitates the exploration of a sustainable alternative to FA that can be utilised as an ASR mitigating SCM in concrete.

There exists another often-overlooked byproduct of the coal industry that could potentially play a role akin to FA in mitigating ASR in concrete. Pond ash (PA) is the waste component of ash produced in coal power plants, typically disposed of in outdoor ash ponds or storage tanks, posing environmental risks [21]. In 2016, global coal combustion ash production was reported at 1221.9 million metric tons (Mt) per year, with only 63.9 % utilised, leaving 544.2 Mt as waste [22]. A 2022 survey indicated that approximately 5.1 million tonnes of ash waste were stored in onsite ponds, awaiting potential reuse [23]. Hence, it is crucial to seek methods to reclaim and reuse this resource, thereby minimising the negative environmental impacts. In this study, reclaimed PA is used with minimal processing to avoid additional environmental impacts from further processing. Due to its outdoor disposal, PA may be susceptible to impurities and moisture contamination. As a result, PA may exhibit significantly different physical and chemical properties compared to FA. Therefore, experimental studies are necessary to establish PA as a viable SCM alternative to FA. A previous study conducted by us demonstrated that PA can effectively mitigate ASR in glass mortar, similar to FA [24]. However, further research is required to evaluate its viability in concrete. The successful utilisation of reclaimed PA in concrete could be a significant step forward in achieving sustainability goals within the construction industry.

Although numerous studies evaluate the physical, mechanical, and durability properties of concrete using waste glass, its adoption in the construction industry remains limited. This hesitance may stem from conflicting results on strength performance and concerns about durability due to ASR. Furthermore, research on the structural applications of glass-added concrete is scarce, especially the behaviour of beams made with GFA concrete. Mustafa et al. [25] tested reinforced concrete beams with GFA for flexure and observed a 10.4 % increase in cracking load at 10 % GFA, and a 5.2 % decrease at 15 % GFA compared to control beams, while ultimate load and deformation showed insignificant changes. This indicates that GFA can be used in steel-reinforced concrete beams up to 15 % without significantly affecting flexural behaviour. However, studies on higher GFA percentages in concrete beams are lacking and crack initiation and propagation were not thoroughly investigated. Hence, this study replaced conventional fine aggregates with up to 40 % GFA in concrete beams and evaluated its effect on the flexural behaviour of the beams. Nevertheless, as discussed earlier, the high utilisation of GFA in concrete can lead to ASR expansion. To mitigate ASR in concrete incorporating GFA, PA was used as the SCM and was compared with FA, building on our previous demonstration of PA's effectiveness in ASR mitigation [24]. Moreover, beams were tested at 28 days and six months to investigate the long-term behaviour of beams with GFA and PA. Along with beams, a comprehensive investigation was conducted to study the compressive, tensile and flexural strengths of the concrete. This study is significant because it investigated the use of two waste materials, GFA and pond ash, in concrete while providing a comprehensive structural assessment. This evaluation underscores the potential of these sustainable materials to deliver robust and reliable construction solutions.

2. Materials and test methods

2.1. Materials

This study utilised ordinary Portland cement (OPC) as the primary cementitious material and commercially available river sand as the main fine aggregate. Crushed waste glass, sourced from "iQRenew" in Queensland, Australia, was incorporated as a sustainable substitute for river sand. Commercially available gravel with a maximum nominal size of 20 mm was used as the coarse aggregate. Additionally, commercially available Class-F fly ash and pond ash from a coal power station in Queensland, Australia, were employed as SCMs to replace OPC partially. The raw materials used in this study are presented in Fig. 1.

Table 1 presents the physical properties of both GFA and river sand. The moisture content, a critical parameter in material analysis, was measured following the standardised procedure outlined in ASTM C566 [26]. Furthermore, the absorption and densities of the materials were assessed following the guidelines given in ASTM C128 [27]. River sand exhibited a significantly higher moisture content and moisture absorption in comparison to GFA.

Fig. 2 provides a visual comparison of the grading between GFA and river sand, illustrating their respective particle size distributions per ASTM C33 specifications [28]. Both the river sand and GFA used in this study conform to the ASTM C33 requirements for fine aggregates. The particle sizes of the cementitious materials were measured using a laser particle size analyser, which showed mean sizes of 15.9 μm for OPC and 15.0 μm for FA. Due to its unrefined nature, PA exhibited a significantly larger mean particle size of 39.9 μm.

2.2. Mix design

The experimental program comprised several mixes with varying percentages of GFA and SCMs, as outlined in Tables 2 and 3. The study was conducted in two stages. In the first stage, a comprehensive investigation was carried out to evaluate the effects of GFA and PA on concrete properties (Table 2). In the second stage, selected GFA percentages and a single PA replacement level were used to assess the flexural behaviour of reinforced concrete (RC) beams (Table 3). The control mix, representing conventional concrete without GFA or PA, was designed to achieve a target 28-day cylinder strength of 30 MPa with a 5 % defective rate. In the first stage, to assess workability and mechanical properties, including compressive strength, splitting tensile strength, and flexural strength, conventional fine aggregates were replaced with GFA in 10 % increments up to 50 %, as detailed in Table 2.

The previous mortar study by the authors evaluated strength development with up to 100 % GFA replacement, increasing the GFA content in 20 % increments [24]. That study found minimal strength reduction up to 60 % GFA, with significant declines beyond that point. Based on these findings, the GFA content in the first-stage concrete study was limited to a maximum of 50 %. To evaluate the effect of PA on GFA concrete, OPC was replaced with PA in 10 % increments up to 30 %, with the GFA level fixed at 50 %. Equivalent binder replacement levels using FA were also prepared to allow comparison with PA. Across all mixes, the total water content and water-to-cement ratio were

Fig. 1. Raw materials; (a) GFA; (b) OPC; (c) PA; (d) FA.

Table 1
Physical properties of GFA and river sand.

Property	Sand	GFA
Moisture content (%)	3.9	1
Water absorption (%)	0.48	0.3
Dry density (kg/m^3)	2627	2438
SSD density (kg/m^3)	2640	2451

maintained at 205 kg/m^3 and 0.44, respectively. Adjustments were made based on aggregate moisture content and absorption data (Table 1) to ensure constant water content between all mixes.

After analysing the mechanical properties of concrete containing GFA and PA/FA in the first stage of the study, selected mix combinations were used for beam casting, as detailed in Table 3. The beam tests focused on 0 %, 20 %, and 40 % GFA replacement levels to evaluate both low and high GFA utilisation. To assess the effect of SCMs, additional beams were prepared by incorporating 20 % PA or FA at each GFA level. While the mechanical property evaluation (Table 2) explored a broader range of GFA content (0–50 %) and PA/FA levels (up to 30 % at 50 % GFA), the beam program was designed to target key combinations. This approach allowed the study to isolate and examine the structural implications of increasing GFA content and the inclusion of SCMs on the performance of concrete beams. Two identical sets of beams were cast

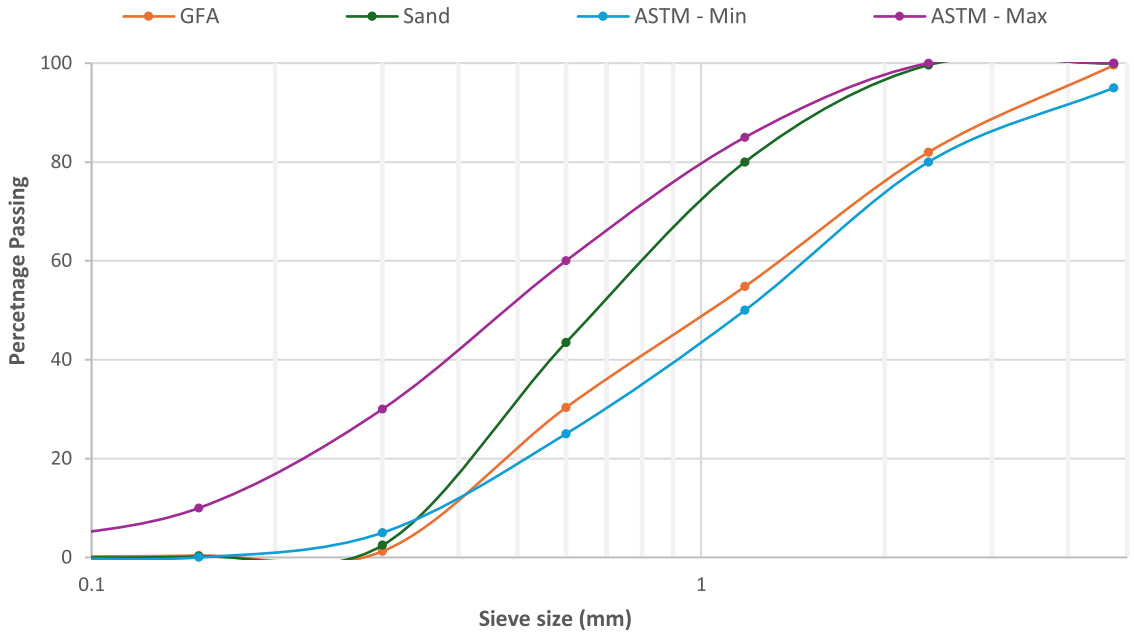

Fig. 2. Particle size distributions.

Table 2
Concrete mix proportions.

Mix designation	Mix Proportions							
	Cement/Binder (kg/m^3)					Fine aggregate (kg/m^3)		
	OPC	Fly ash	Fly ash %	Pond ash	Pond ash %	Sand	GFA	GFA %
0GFA - 0FA - 0PA	466					581	0	0
10GFA - 0FA - 0PA	466					523	58	10
20GFA - 0FA - 0PA	466					465	116	20
30GFA - 0FA - 0PA	466					407	174	30
40GFA - 0FA - 0PA	466					349	232	40
50GFA - 0FA - 0PA	466					291	291	50
50GFA - 10FA - 0PA	419	47	10			291	291	50
50GFA - 20FA - 0PA	373	93	20			291	291	50
50GFA - 30FA - 0PA	326	140	30			291	291	50
50GFA - 0FA - 10PA	419			47	10	291	291	50
50GFA - 0FA - 20PA	373			93	20	291	291	50
50GFA - 0FA - 30PA	326			140	30	291	291	50

Table 3
Concrete mixes for evaluating the flexural behaviour of beams.

Beam designation	Mix Proportions							
	Cement/Binder (kg/m^3)					Fine aggregate (kg/m^3)		
	OPC	Fly ash	Fly ash %	Pond ash	Pond ash %	Sand	GFA	GFA %
0GFA - 0FA - 0PA	466					581	0	0
20GFA - 0FA - 0PA	466					465	116	20
40GFA - 0FA - 0PA	466					349	232	40
0GFA - 20FA - 0PA	373	93	20			581	0	0
20GFA - 20FA - 0PA	373	93	20			465	116	20
40GFA - 20FA - 0PA	373	93	20			349	232	40
0GFA - 0FA - 20PA	373			93	20	581	0	0
20GFA - 0FA - 20PA	373			93	20	465	116	20
40GFA - 0FA - 20PA	373			93	20	349	232	40

using these mix designs: one tested at 28 days, and the other at six months. The six-month testing aimed to assess the long-term effects of GFA and PA utilisation, providing insight into the durability and structural performance of these sustainable concrete mixes by comparing beams with and without SCMs over time.

Slump tests were conducted on fresh concrete per AS 1012.3.1 [29] to evaluate workability. A cone (300 mm high; 200 mm bottom and 100 mm top diameters) was placed on a clean, smooth steel base. Concrete was added in three layers, each compacted 25 times with a standard rod. After levelling, the cone was lifted vertically, and the slump was measured as the reduction in concrete height. It should be noted that the slump of GFA mixes was deliberately kept low to avoid excessive workability when PA or FA was added. The combined use of GFA and SCMs can significantly increase slump, leading to segregation as shown in 3.1. In practical applications, admixtures can be used to improve workability, especially for pumping.

2.3. Testing for mechanical properties of concrete

Cylinder specimens (100 mm × 200 mm) were cast per AS 1012.9 [30] standard to evaluate compressive strength. Three cylinders per mix were poured in three layers and compacted with a vibrating table. After demoulding at 24 h, specimens were cured at 100 % humidity and tested at 28 days and six months using a universal testing machine at a rate of 20 MPa/min. Splitting tensile strength was determined according to AS 1012.10 [31]. Three specimens per mix were tested, with diameters measured at three points and lengths averaged from at least two measurements. Hardboard bearing strips were placed between platens, and the load was applied at 1.5 MPa/min until failure; the maximum force was recorded. Flexural strength was assessed using simple beams (100 mm × 100 mm, 350 mm long with a 300 mm effective length) per AS 1012.11 [32]. Two beams per mix were tested. First, any surface debris was removed, and then the beam was centred on rollers. A seating load up to 100 N was applied, followed by a continuous load at 2 kN/min. The maximum load was recorded, and the average width and depth at the failure section were measured to calculate the modulus of rupture.

2.4. Flexural test on steel-reinforced concrete beams

2.4.1. Design and beam specimen preparation

A total of 18 steel-reinforced concrete (RC) beams were cast and tested under three-point bending to investigate the flexural behaviour of concrete incorporating GFA and PA/FA. All beams had cross-sectional dimensions of 100 mm × 250 mm and a total length of 1400 mm (Fig. 3). An effective span of 1300 mm was used for testing, with 50 mm at each end of the 1400 mm beam reserved for seating on the supports. The design of the beams was carried out according to Eurocode 2 (EC2) [33], ensuring flexural failure governed the response rather than shear failure. Longitudinal reinforcement consisted of four deformed steel bars with 10 mm diameter, positioned equally at the top and bottom faces, while 10 mm diameter stirrups were provided at 150 mm spacing. All

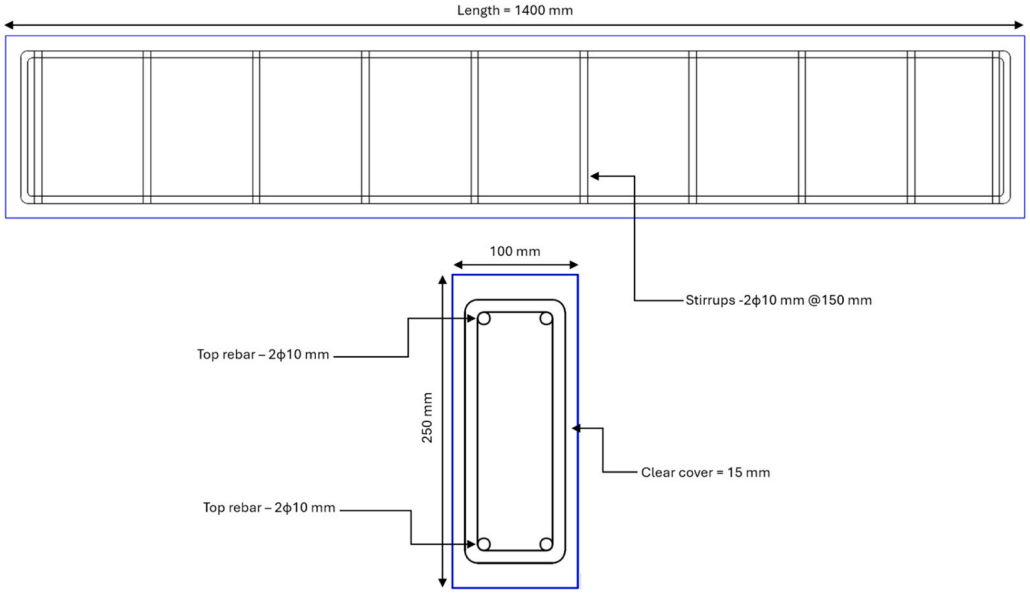

Fig. 3. Beam geometry and reinforcement details.

reinforcement bars, including the top, bottom, and stirrups, were made from the same steel with a characteristic yield strength of 500 MPa. This reinforcement configuration corresponded to a longitudinal reinforcement ratio of 1.26 % and a stirrup ratio of 1.047 %. The shear span ratio was maintained at 3.04 for all beams. The beams were designed to promote flexural failure by ensuring a relatively high shear span-to-depth ratio of 3.04, which is well above the typical threshold of 2.0 that differentiates shear-dominated behaviour from flexural behaviour. Additionally, the stirrup ratio of 1.047 % and the use of closely spaced ϕ10 stirrups at 150 mm provided sufficient shear reinforcement to prevent premature shear failure. This configuration ensures that the beams fail in flexure, as intended, with yielding of the longitudinal reinforcement governing the ultimate load response.

The relatively small beam dimensions used in this study were selected to enable a material-focused evaluation of flexural behaviour, cracking characteristics, and serviceability under controlled laboratory conditions. While small-scale specimens may not fully replicate the load distribution and crack patterns of full-size members, such scaled testing is widely accepted in early-stage research to investigate fundamental material responses [34,35]. However, it is acknowledged that the size effect, which refers to the reduction in nominal strength as structural size increases, can influence parameters such as cracking load, deflection, and failure mode, particularly in shear-critical members. As noted by Jin et al. [36], geometrically scaled specimens may exhibit different stress redistribution and failure mechanisms due to variations in energy dissipation and crack propagation. Although the present study focuses on flexure-dominant behaviour, future investigations involving full-scale or larger beams are recommended to verify the applicability of the observed performance trends to real-world structural elements.

Fabricated steel cages were positioned inside well-lubricated moulds, with a 15 mm concrete cover to the main reinforcement bars, as illustrated in Fig. 4(a). The relatively small cover thickness was adopted to accelerate potential environmental effects on reinforcement over the six-month curing period, facilitating an early assessment of material durability. Concrete was carefully poured and compacted using a poker vibrator to minimise segregation while ensuring adequate consolidation (Fig. 4(b)). After demoulding at 24 h, specimens were stored in a controlled environment until testing at 28 days and six months.

2.4.2. Loading and instrumentation

A loading frame equipped with a 300 kN load cell attached to a hydraulic loading system was utilised to apply an incrementally increasing load to the beams until failure, as depicted in Fig. 4(c). A roller placed beneath the load cell facilitated the transfer of the load to the top surface at the midpoint of the beam. The three-point bending setup was chosen for its favourable conditions for flexural failure. A laser displacement sensor was positioned underneath the beam at the midpoint to measure the mid-span deflection of the beam. A data logger was used to record both applied load and mid-span deflection. The loading was applied manually using a hydraulic system, with the rate controlled visually by monitoring load and time data collected from the data logger to ensure a slow and consistent loading process. Additionally, digital image correlation (DIC) was employed to investigate the crack propagation behaviour of the beams. One side of the beam was first painted white, and small black dots were drawn using ink and a roller provided in the DIC kit. A high-resolution camera (ISM-LENS-GP013) connected to an Imetrum System Controller (SC-1) was used to record the response of the beam during testing. The videos were analysed using Video Gauge 5.4.4 (Imetrum Ltd.) and ZEISS Correlate (Carl Zeiss AG), both commercial DIC software packages, to generate strain maps and quantify crack propagation.

3. Results and discussion

3.1. Workability

The workability of fresh concrete was evaluated through slump tests, and the influence of GFA content and SCM incorporation is presented in Fig. 5. Increasing GFA content led to a gradual reduction in workability (Fig. 5(a)), with minimal impact up to 30 % GFA content. This trend has been previously reported [37–39] and is primarily attributed to the angular and irregular morphology of GFA particles.

As revealed by SEM images (Fig. 6), GFA granules exhibit sharp ridges and rough surfaces, which increase inter-particle friction compared to the smoother, rounded grains of natural river sand, thereby reducing the fluidity of fresh concrete. This hypothesis is further corroborated by the findings of Surendran and Akhas [40], who demonstrated that processing waste glass into smoother, cubical shapes led to a measurable improvement in workability by approximately 10 %. Their results affirm that angularity plays a dominant role in governing the workability of GFA concrete and that eliminating angular features can partially restore the flow characteristics impaired by crushed glass.

The incorporation of PA and FA significantly enhanced the workability of GFA concrete compared to OPC-only mixes (Fig. 5(b)). SEM analysis (Fig. 7) shows that PA and FA particles are predominantly spherical and smooth, reducing internal friction and improving particle packing. This phenomenon is consistent with previous findings regarding the effect of fly ash on concrete rheology [41,42]. Furthermore, PA mixes demonstrated superior workability compared to FA

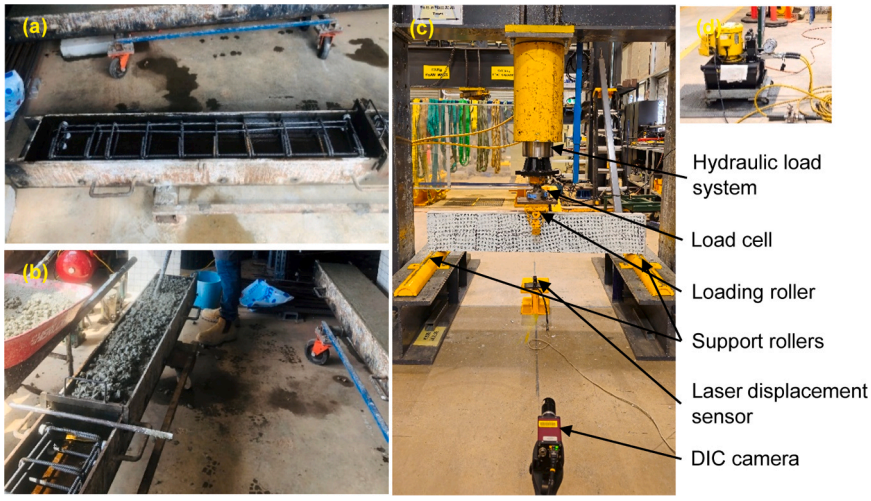

Fig. 4. (a) steel reinforcement cage inside the formwork; (b) concrete pouring and compaction; (c) Load setup and instrumentation; (d) hydraulic pump unit.

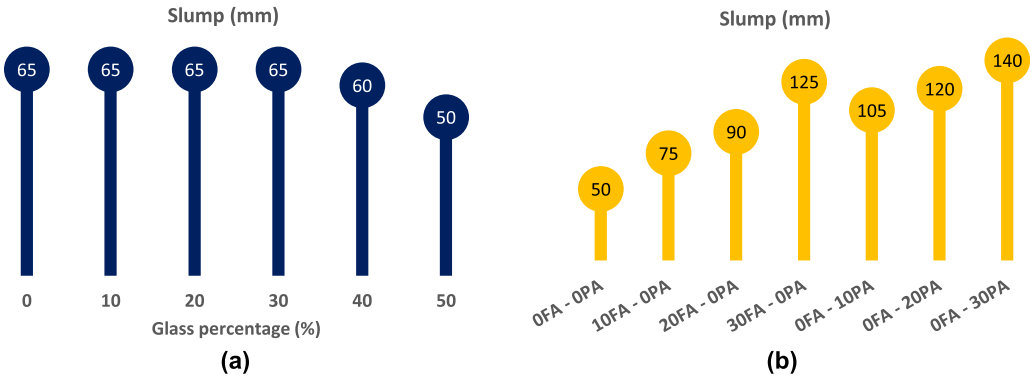

Fig. 5. Impact on the slump; (a) by increasing GFA; (b) by replacing OPC with PA/FA for 50 % GFA concrete.

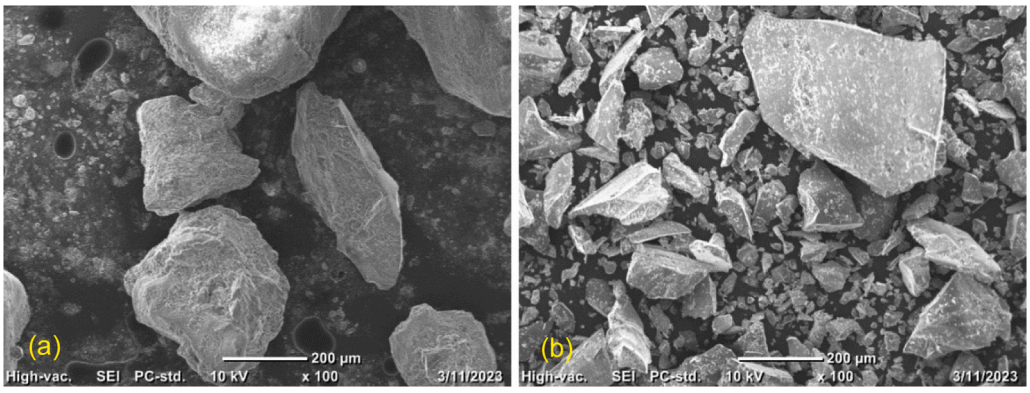

Fig. 6. SEM images of (a) river sand, (b) GFA.

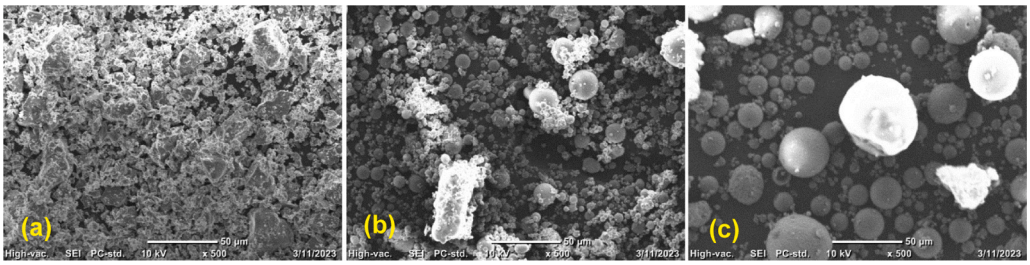

Fig. 7. SEM images of (a) cement, (b) FA, (c) PA.

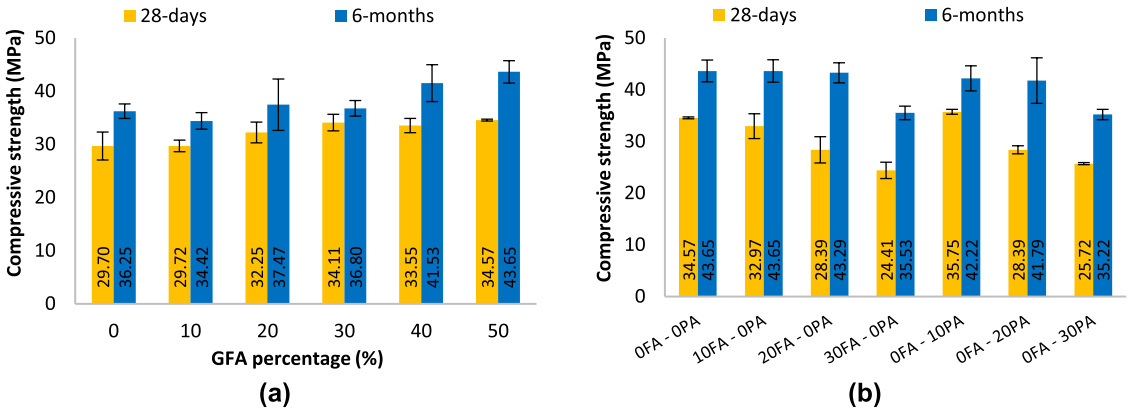

Fig. 8. Impact on compressive strength; (a) by increasing GFA; (b) by replacing OPC with PA/FA for 50 % GFA concrete.

mixes. Although FA particles are also spherical, they exhibited greater agglomeration, whereas PA particles were more dispersed, minimising clustering and further improving flowability. These observations suggest that PA can offer not only comparable pozzolanic reactivity but also better fresh-state workability relative to FA when combined with high levels of GFA content.

3.2. Mechanical properties of GFA concrete

3.2.1. Compressive strength

The influence of GFA incorporation on the compressive strength of concrete at 28 days and six months is shown in Fig. 8(a). The results indicate a gradual increase in 28-day compressive strength with increasing GFA content, reaching a 16.4 % improvement at 50 % GFA. Similar strength enhancements with GFA have been observed in prior studies [37,43]. Previous researchers, such as Jamellodin et al. [43], attributed strength improvements to enhanced bonding at the GFA-cement paste interface. However, experimental observations from the prior mortar study conducted by the authors challenge this explanation [24]. In that study, compressive strength increases were negligible when coarse aggregates were removed, suggesting that the strength gain in GFA concrete arises primarily from mechanical interlocking between the irregular GFA granules and the surrounding coarse aggregates, rather than interfacial bond improvements. At six months, the increasing trend became more pronounced, with a 20.4 % strength enhancement at 50 % GFA.

This delayed strength development is consistent with the potential pozzolanic activity of waste glass. Previous investigations [44–46] reported that the amorphous silica present in waste glass can react with calcium hydroxide [$Ca(OH)_2$], resulting in additional calcium silicate hydrate (C-S-H) formation at the aggregate interface (ITZ). This behaviour was observed at six months in our previous mortar study, which demonstrated enhanced bonding at the ITZ between GFA particles and the cement matrix [20,24], as shown in Fig. 9. The improved ITZ likely increases the concrete's resistance to crack initiation and propagation. This secondary reaction likely improves the microstructure over time, contributing to the long-term strength gain observed in GFA concrete.

Fig. 10 shows the failure modes of the tested cylinders under compression. The inclusion of 50 % GFA improved the concrete's resistance to compressive stress, as evidenced by significantly fewer cracks compared to the control specimen at 28 days. At six months, the control cylinder also exhibited fewer cracks than its 28-day counterpart, reflecting strength development over time. Similarly, the six-month specimen with 50 % GFA demonstrated crack patterns comparable to its 28-day equivalent, reinforcing the trend of enhanced compressive behaviour observed in the strength results.

The effect of replacing OPC with PA or FA on compressive strength for 50 % GFA concrete is shown in Fig. 8(b). At 10 % replacement levels, PA marginally improved strength relative to the OPC-only mix, whereas FA resulted in a slight strength reduction. At 20 % and 30 % replacement, both PA and FA caused progressive strength losses, although PA consistently performed better than FA. This strength reduction is primarily attributed to the dilution of CaO, as both PA and FA possess lower calcium contents compared to OPC [24]. The superior performance of PA relative to FA is linked to its higher alumino-silicate content (Al_2O_3 and SiO_2), which enhances pozzolanic activity and promotes the formation of additional C-S-H and calcium aluminate hydrate (C-A-H) phases [47]. These secondary products densify the matrix and partially offset strength reductions caused by reduced cement content. At six months, the compressive strength differences between the OPC, PA, and FA mixes were diminished (Fig. 8(b)). At 10 % and 20 % replacement levels, both PA- and FA-incorporated concretes achieved strengths comparable to the OPC control, indicating that pozzolanic reactions compensated for initial dilution effects over time. However, at 30 % replacement, significant strength reductions were still observed, with PA and FA mixes showing 19.3 % and 18.6 % reductions, respectively. Although FA has significantly finer particle sizes than PA, PA still achieved comparable performance to FA in both short- and long-term strengths, demonstrating the viability of using pond ash as a substitute for FA in terms of strength performance. The 28-day tested cylinders also demonstrate superior compressive resistance with PA, as the PA specimens exhibited fewer cracks than the FA specimens. Notably, the PA mix showed less cracking than the 28-day control as well, aligning with the observed compressive strength results. At six months, both FA and PA specimens displayed similar failure patterns, reflecting the comparable strength development observed in the test data.

Despite the overall increasing trend in compressive strength, some fluctuations were observed at intermediate GFA levels, particularly at six months. These variations may arise from the heterogeneous nature of waste glass, which includes inconsistencies in particle shape, size distribution, and local packing density. Such irregularities can influence the microstructure of the concrete and promote the formation of micro voids, ultimately affecting strength development [48,49]. Additionally, minor inconsistencies in mixing, compaction, or internal moisture distribution may become more pronounced over time, particularly in concretes containing angular or non-uniform particles like GFA. Similar variability has been reported in previous studies, indicating that such strength fluctuations are within the expected performance range of concrete made with recycled materials [37].

3.2.2. Tensile strength

Fig. 11(a) shows that splitting tensile strength increases steadily as the proportion of GFA rises. At 50 % GFA replacement, tensile strength is about 16.5 % higher than in the control mix. A similar upward trend at lower GFA levels was observed by Abdallah and Fan [14] and Borhan [50]. The same mechanism that raised compressive strength at higher GFA levels, namely increased aggregate interlocking, also appears to

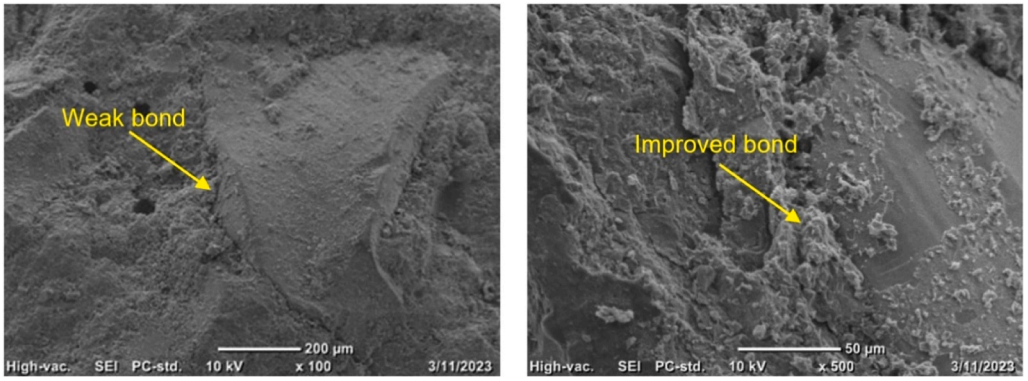

Fig. 9. SEM images of: (a) 28-day mortar with 100 % GFA; (b) 91-day mortar with 100 % GFA [20].

Fig. 10. Failure modes of tested cylinders for compression: 28-day cylinders; (a) 0 GFA-0FA-0PA, (b) 50GFA-0FA-0PA, (c) 50GFA-20FA-0PA, (d) 50GFA-0FA-20PA, and six-month cylinders; (e) 0GFA-0FA-0PA, (f) 50GFA-0FA-0PA, (g) 50GFA-20FA-0PA, (h) 50GFA-0FA-20PA.

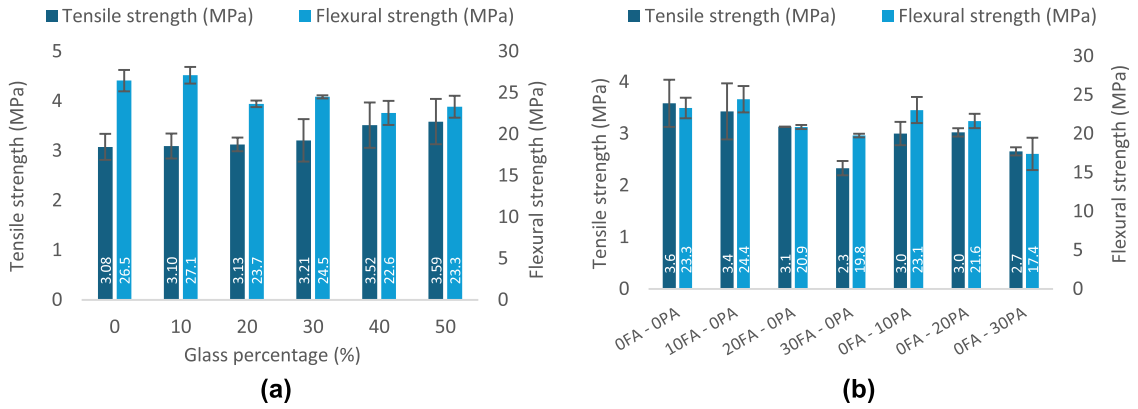

Fig. 11. Impact on tensile and flexural strength; (a) by increasing GFA; (b) by replacing OPC with PA/FA for 50 % GFA concrete.

underlie the observed increase in tensile strength. From 0 % to 30 % GFA, the increase in tensile strength is relatively modest despite the incremental rise in GFA content. This is likely because, at low replacement levels, the quantity of GFA particles is insufficient to develop significant mechanical interlocking throughout the matrix. However, at 40 % and 50 % GFA, a more noticeable increase in tensile strength is observed. This can be attributed to the higher concentration of angular GFA particles, which enhances inter-particle contact and interlocking. As the amount of GFA increases, the likelihood of overlapping and bridging between adjacent particles also rises, allowing the aggregate network to resist tensile cracking more effectively. This densified internal structure contributes to better tensile stress distribution and explains the sharper gains in tensile strength at higher GFA replacement levels.

Fig. 11(b) presents the effect of PA and FA on tensile strength for concrete containing 50 % GFA. Replacing 10 % of OPC with PA or FA lowers tensile strength relative to the 100 % OPC mix; PA causes a slightly larger reduction than FA at this level. At 20 % replacement, the two SCMs produce almost identical strength losses. At 30 % replacement, PA outperforms FA: tensile strength in the PA mix is only 11.5 % lower than in its 10 % counterpart, whereas the FA mix shows a 32 % drop from its 10 % level. This behaviour confirms that PA provides a more stable tensile-strength response than FA at higher replacement levels.

3.2.3. Flexural strength

Fig. 11(a) illustrates that flexural strength, expressed as modulus of rupture, declines almost linearly as the GFA level increases. The control mix attains the highest value, while the 50 % GFA mix gives the lowest. Comparable reductions were documented by Limbachiya [51], Taha and Nounu [52] and Sharifi et al. [53]; each study attributed the decline in flexural capacity to the smooth, flat surfaces of crushed glass, which inhibit mechanical interlock with the cement matrix, and to microcracks in GFA that were generated during the crushing process. Fig. 11(b) shows the influence of replacing OPC with PA or FA in concrete containing 50 % GFA. At a 10 % replacement level, flexural strength remains largely unchanged, although PA is marginally lower than FA. When the replacement ratio reaches 20 %, both SCMs reduce strength relative to the control, with PA performing slightly better than FA. At 30 % replacement, PA falls below both the FA and OPC mixes. The progressive strength decline is mainly caused by the dilution of the cement paste, while the elevated workability of the PA and FA mixes adds further risk. Highly fluid concrete can segregate if consolidation is insufficient, producing weak planes that reduce flexural capacity [41], which explains the lower performance of PA, as it exhibited higher workability than FA.

With the mechanical properties of the GFA concretes established, the discussion now turns to the flexural performance of the steel-reinforced concrete beams, with particular attention to crack propagation as well as the load-deflection response.

3.3. Flexural behaviour of steel-reinforced concrete beams

3.3.1. Failure mode and crack propagation

DIC was used to map surface strains and track crack development in all beams, as illustrated in Figs. 12 and 13. Unlike manual crack-marking methods, DIC provides full-field strain data that allows each crack to be linked precisely to the corresponding load step. For every beam, the first visible crack formed at mid-span, where the bending moment and tensile stress are highest. As the load increased, additional cracks gradually developed in the direction of the supports, with all cracks widening and extending further into the compression zone. Mid-span cracks remained almost vertical, reflecting pure flexure, whereas cracks closer to the supports displayed increasing inclination because shear stresses contributed to diagonal tension. As the load continued to increase, the beams eventually failed in flexure, with no further load increase observed.

At 28 days, the beam with 20 % GFA showed earlier crack initiation and more rapid crack growth than the control without GFA, whereas the

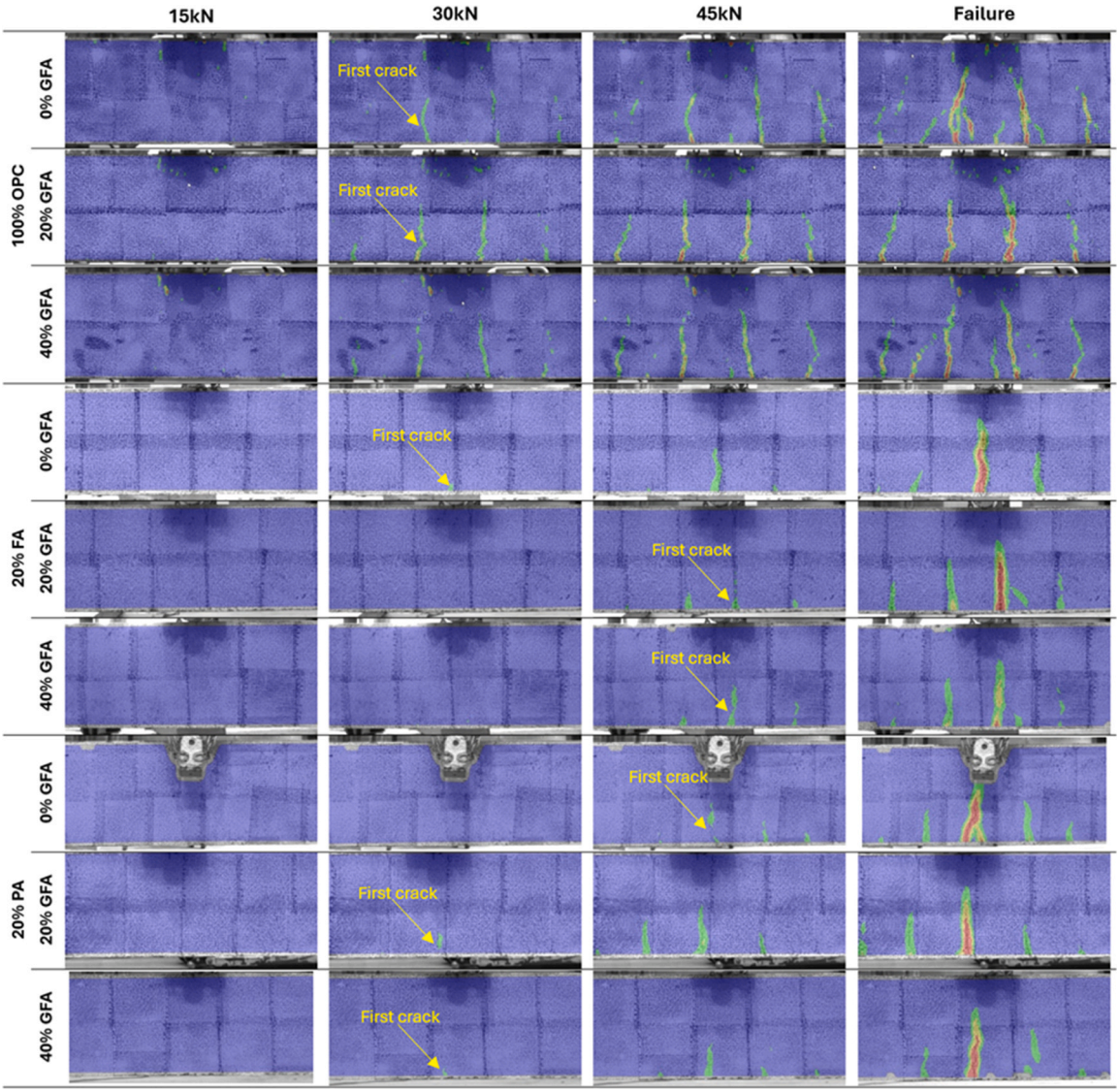

Fig. 12. DIC strain maps for crack propagation analysis of 28-day beams (Access the animation).

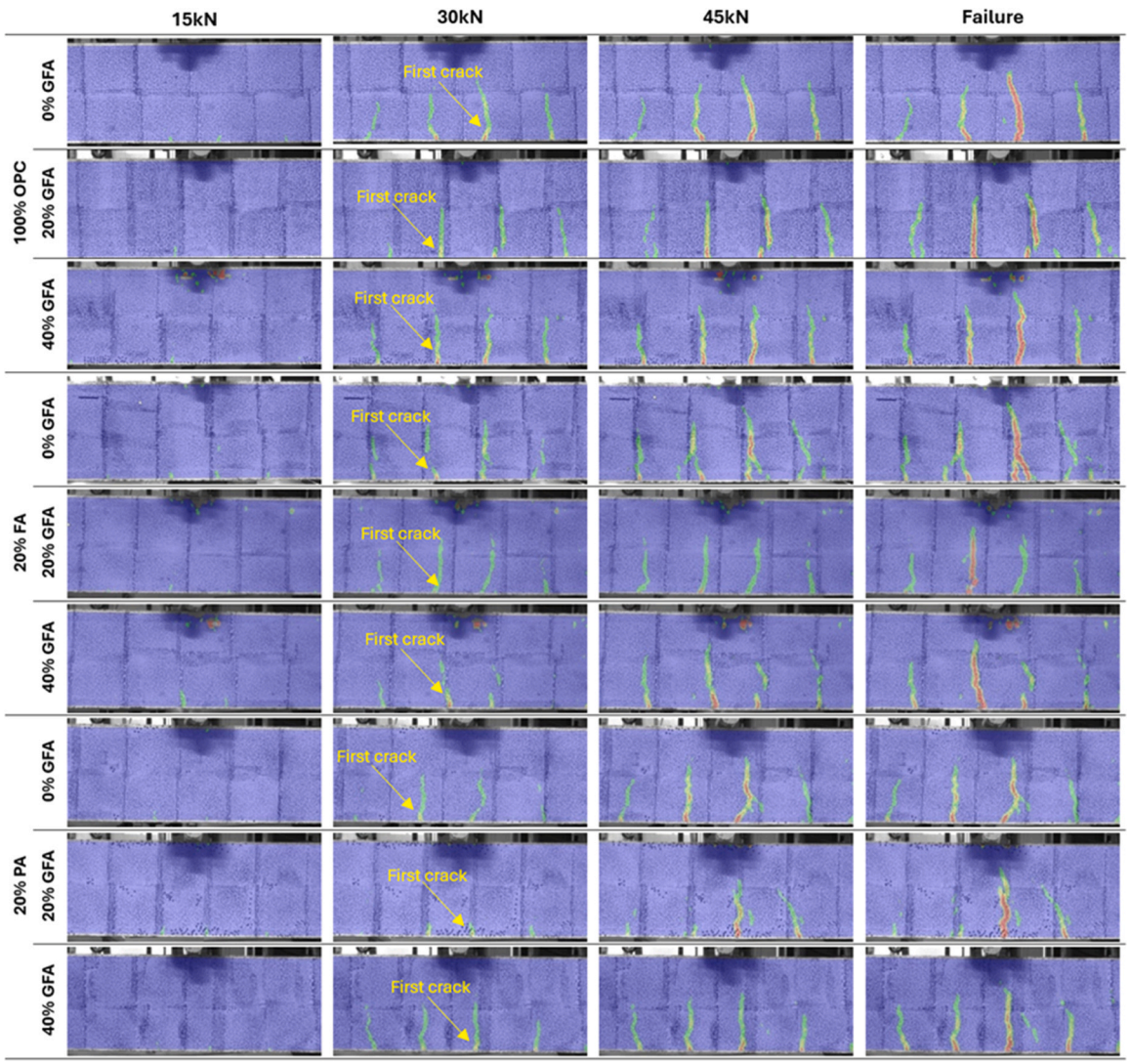

Fig. 13. DIC strain maps for crack propagation analysis of six-month beams (Access the animation).

40 % GFA beam exhibited slightly better resistance than the 20 % level, as can be observed in Fig. 12. The GFA mixes, however, developed wider cracks than the control once the load exceeded about 40 kN, which mirrors the flexural-strength reductions discussed in 3.2.3. Introducing 20 % PA or FA improved crack resistance across all GFA levels; the PA and FA beams displayed fewer and narrower cracks than the corresponding OPC beams, although their final failure was more abrupt and therefore less ductile than OPC counterparts.

As shown in Fig. 13, at the six-month test age, the behaviour changed. Both 20 % and 40 % GFA beams performed similarly to the control, indicating an age-related improvement in crack resistance with GFA. Adding 20 % PA further reduced crack widths and slowed crack propagation relative to both OPC and 20 % FA beams for every GFA level up to about 45 kN. The FA beams also improved over the OPC beams, but to a slightly lesser extent. In contrast with the 28-day results, failure of the PA and FA beams at six months was less sudden, suggesting that the pozzolanic reaction of the SCMs had enhanced the tensile-zone microstructure and moderated crack growth.

Although visual observation of crack propagation offers some insight into cracking behaviour, it is insufficient for a comprehensive assessment. Therefore, the DIC data were further analysed to quantify the load at which the first crack appeared and to track the progression of the principal crack as the load increased. These measurements provide a more robust and objective basis for evaluating and comparing the cracking performance of the beams.

3.3.2. *Crack Initiation Load*

The load at which the first crack appeared is presented in Fig. 14. The data indicate that increasing GFA content led to the initial crack forming earlier, specifically at 28 days. This behaviour can be explained by the smooth, flat surfaces and pre-existing microcracks in the GFA, which contributed to the reduction in flexural strength in GFA concrete at this stage. However, at six months, an opposite trend emerged. The control beam with 0 % GFA and 100 % OPC exhibited a reduction in the crack initiation load from 28 days to six months, suggesting deterioration over time. In contrast, beams with 20 % GFA performed slightly better at six months compared to 28 days, while beams with 40 % GFA showed a significant improvement at the six-month mark. This highlights GFA's ability to enhance the beam's resistance to environmental degradation over a longer period, compensating for the initial weakness and contributing to the durability of the concrete.

At 28 days, incorporating both PA and FA significantly delayed crack initiation, particularly in beams with 20 % and 40 % GFA. This delay is attributed to improved compaction from increased workability and reduced thermal cracking. It has been demonstrated that FA lowers heat generation by moderating the hydration reaction [54], thereby mitigating thermal cracking. Similar effects are observed with PA, which, due to its high workability and low CaO content, contributes to higher

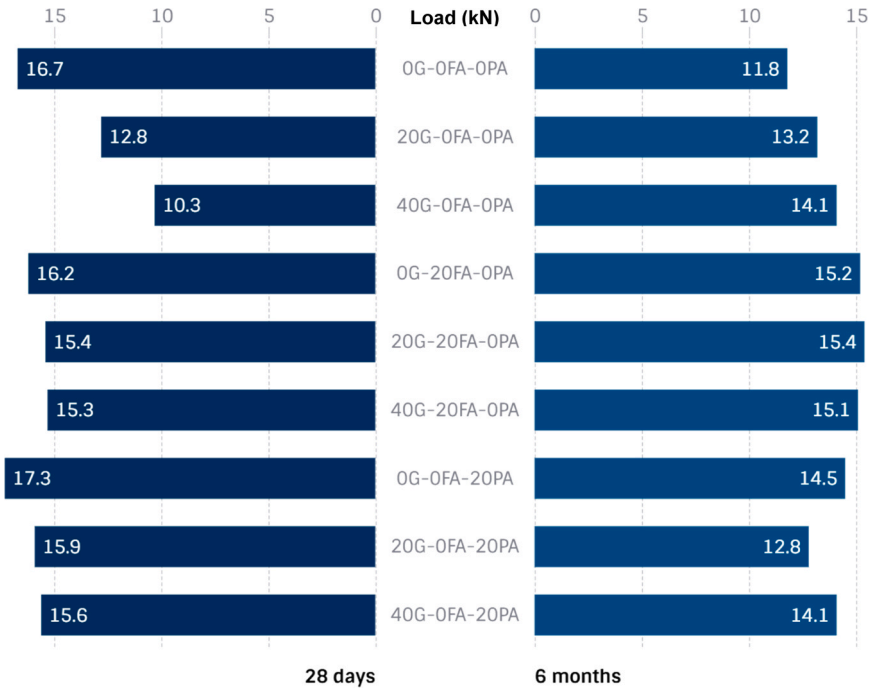

Fig. 14. Crack Initiation Load.

cracking loads. By six months, PA beams exhibited behaviour similar to OPC beams, while FA beams performed slightly better than their OPC counterparts. Both PA and FA outperformed the OPC control without GFA. This improvement is attributed to the pozzolanic materials' ability to enhance the microstructure through additional C-S-H formation, which improves resistance to environmental effects [55]. However, PA beams showed lower crack initiation loads than FA beams across all GFA levels at six months. The lower reactivity of PA may be due to its larger particle size, which results in weaker interaggregate bonds. Despite this, both PA and FA provided better serviceability in GFA-concrete beams compared to OPC.

3.3.3. *Load vs crack width analysis*

Fig. 15 plots crack width against load for all beams, providing a direct measure of serviceability. For each beam, the width of the first visible crack, which was typically the most critical, was tracked and measured as the load increased using DIC data to generate consistent crack width versus load curves. In the OPC series at 28 days, the inclusion of GFA increased the crack width: beams with 20 % and 40 % GFA developed wider cracks than the control as the load rose. This response is attributed to the smooth faces of crushed glass, which bond less effectively with the cement matrix, and to the greater friability of glass compared with natural sand [52,56]. At six months, every beam displayed larger crack widths than its 28-day counterparts in the OPC series. However, in contrast to the 28-day results, where increasing GFA content led to wider cracking, the six-month results revealed a reduction in crack widths with higher GFA levels. This behaviour can be explained by two contributing factors. The improved bond between GFA and the cement matrix, resulting from the pozzolanic activity of GFA, is a key factor contributing to the reduced crack widths observed in the six-month beams with higher GFA content. Moreover, in an electrochemical corrosion study, Wei et al. [57] observed that higher GFA content in concrete cylinders reduced rebar corrosion, primarily due to decreased concrete porosity. In addition, previous research has shown that GFA granules, being impermeable, act as physical barriers that limit the ingress of water and ions, thereby enhancing durability [58,59]. These factors may also contribute to the reduced crack widths observed in beams with higher GFA levels at six months. Hence, the larger crack widths observed in the six-month OPC beams may be reasonably attributed to the slight degradation of the steel reinforcement over time. Although no visual evidence of corrosion was identified, the consistent increase in cracking in all OPC beams, coupled with the reduction in cracking in GFA-containing beams, supports this hypothesis. Furthermore, the compressive strength results show no indication of material degradation in the concrete matrix itself, as strengths increased at six months across all mixes. Therefore, in the absence of concrete deterioration, reinforcement degradation remains the most plausible explanation for the observed long-term cracking behaviour.

At 28 days, both PA and FA markedly reduced crack widths at every GFA level relative to OPC counterparts. PA achieved the narrowest cracks for the 0 % and 20 % GFA mixes, whereas FA gave similar performance across all GFA contents. The benefit is linked to the higher workability of the PA and FA concretes (Fig. 5(b)), which promotes better consolidation, closer aggregate packing and fewer voids. Lower peak hydration temperatures provided by the SCMs further limit thermal cracking during early curing. The six-month data confirm that PA and FA continue to enhance crack resistance. All PA and FA beams exhibited smaller crack widths than the corresponding OPC counterparts at the same age. FA outperformed PA in the 0 % and 20 % GFA mixes, a difference that reflects the finer particle size and higher reactivity of fly ash, but both SCMs produced substantial gains over OPC. The continued improvement is attributed to microstructural densification that results from ongoing pozzolanic reactions, which fill pores with additional C-S-H. As with the OPC mixes, raising the GFA content reduced crack widths in the PA and FA beams at six months. This outcome can be attributed to the combined effects of the pozzolanic activity of GFA and the reduced porosity and moisture ingress due to the impermeable nature of glass particles, as discussed above.

3.3.4. *Load vs deflection behaviour of concrete beams*

Fig. 16 presents the curves that relate load to mid-span deflection for every beam at 28 days and six months. All curves follow a similar profile, which indicates that neither GFA nor the two SCMs caused major changes in overall flexural response. Subtle differences emerge, however, when characteristic points are compared. These points include the load at first yield of the tensile steel, the ultimate load, the initial elastic

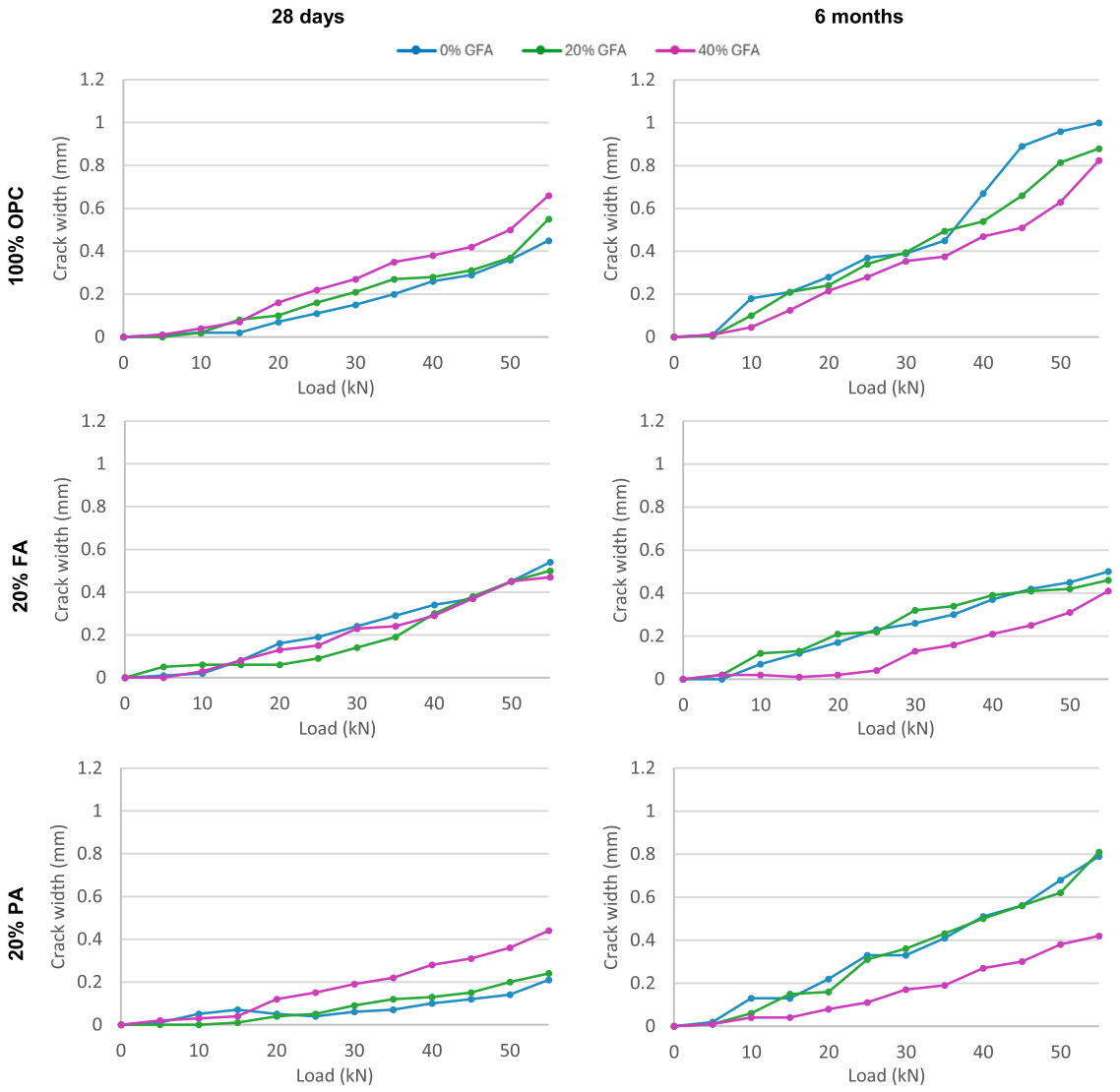

Fig. 15. Load (kN) vs crack width (mm) plots created by the data obtained from DIC.

slope, and the total area under each curve. Table 4 lists the numerical values, and Fig. 17 illustrates them, providing the basis for the more detailed discussion that follows on yield load, ultimate capacity, stiffness, ductility, and energy absorption.

3.3.4.1. Yield load. The yield load was identified on each load-deflection curve as the point where the initially linear response began to deviate, indicating the onset of yielding in the tensile reinforcement [60]. These values are illustrated in Fig. 17(a). In the OPC series at 28 days, replacing sand with 20 % or 40 % GFA did not alter the yield load relative to the 0 % GFA beam, which shows that early-age reserve capacity is governed mainly by steel. After six months, all three OPC mixes displayed a modest decline, averaging about 5 %, even though compressive strength had risen.

Replacing 20 % of OPC with PA or FA altered the short-term response. At 28 days, beams with 0 and 20 % GFA, and both SCMs recorded yield loads that were slightly below their OPC counterparts, reflecting the lower early-age compressive strength of the PA and FA mixes. By six months, this shortfall had almost vanished because continuing pozzolanic reactions densified the compression zone and strengthened the matrix. A different pattern emerged when GFA content reached 40 %. Both PA and FA produced yield loads marginally higher than the OPC beam, with 40 % GFA at both ages. The improvement may arise from two complementary mechanisms. First, the high GFA content lowers permeability and therefore slows moisture and chloride ingress, limiting beam degradation. Second, the pozzolanic reactivity of the supplementary materials and GFA refines the pore network [24,61]. In the long term, FA performed slightly better than PA at every GFA level, an outcome linked to the finer particle size of FA. Finer particles provide a larger reactive surface, leading to greater microstructural densification, whereas the coarser PA particles react more slowly and thus deliver a smaller increase in yield load [24].

3.3.4.2. Ultimate failure load. The ultimate failure load was taken as the highest load recorded on each curve after the reinforcement had yielded, as illustrated in Fig. 17(b). Across the full matrix of mixes, the values at 28 days and six months fell within a narrow band. A single divergence appeared at 28 days for the beams that combined 40 % GFA with either PA or FA; these specimens carried a slightly higher ultimate load than the corresponding OPC beam. The gain is linked to reduced thermal cracking and superior compaction produced by the more workable pozzolanic concretes, both of which help preserve the compression zone until the reinforcement reaches full plasticity.

Apart from this modest benefit, neither GFA content, binder replacement, nor curing age produced a significant change, especially in six-month beams. This limited variation is expected in flexure-dominant

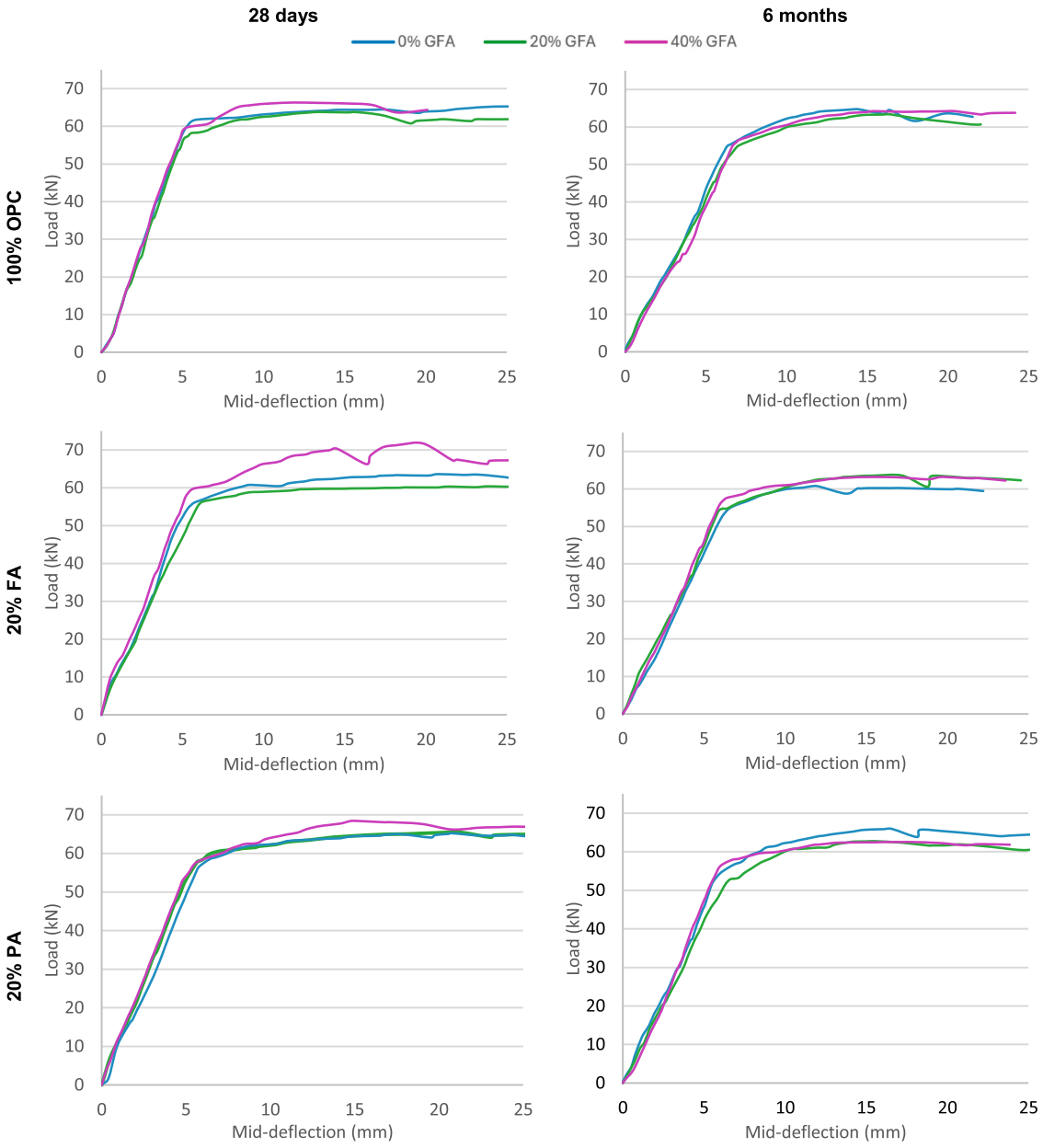

Fig. 16. Deflection (mm) vs load (kN) plots.

reinforced concrete beams, where failure occurs after yielding of the steel reinforcement. Once yielding begins, the contribution of concrete strength becomes secondary, as the beam's load-carrying capacity is governed primarily by the plastic hinge mechanism formed in the steel [62]. Therefore, variations in concrete composition, such as GFA or PA content, do not significantly influence the ultimate load. Most importantly, the use of alternative waste materials did not adversely affect the ultimate failure capacity of the beams, reinforcing their suitability for use in structural concrete applications.

3.3.4.3. Flexural stiffness. Flexural stiffness for each beam was calculated from the slope of the initial straight segment of the load-deflection curve. These values are plotted in Fig. 17(c). In the OPC series at 28 days, increasing GFA from 0 % to 40 % produced only minor changes, confirming that early-age stiffness depends mainly on the elastic modulus of the concrete matrix, which was similar across those mixes. However, by six months, a noticeable reduction in stiffness was observed in all OPC beams. While the concrete compressive strength continued to increase over time, the reduction in stiffness may be attributed to the cumulative effects of internal microcracking, drying shrinkage, reduced bond efficiency between concrete and reinforcement, and potential early-stage reinforcement degradation due to environmental exposure. Drying shrinkage, in particular, is common in all concrete elements and can introduce internal tensile stresses that weaken the bond and induce microcracking, even in the absence of external loading [63]. Although no direct evidence of corrosion was observed, the uniform reduction across all OPC beams suggests that some early deterioration mechanism may have compromised stiffness. The beams were stored in a temperate climate with daily temperature fluctuations ranging from below 5 °C at night to above 20 °C during the day. This thermal cycling, combined with ambient humidity, may have further contributed to internal microcracking or degradation of the concrete and reinforcement. This interpretation aligns with previous studies indicating that stiffness degradation in ageing RC elements can result from bond deterioration, shrinkage effects, and microstructural changes [64,65].

Incorporating PA or FA led to lower beam stiffness at 28 days

Table 4
Experimental and theoretical results.

Beam	Age	Compressive strength (MPa)	First crack (kN)	Slope (kN/mm)	Yield load (kN)	Ultimate load (kN)	Yield deflection (mm)	Ultimate deflection (mm)	Displacement ductility (mm/mm)	Area under curve (kN.mm)	$P_{0.3Cr}$ (kN)	$P_{m.def.}$ (kN)	$M_{cr,exp}$ (kNm)	$M_{u,exp}$ (kNm)	$M_{cr,theo}$ (kNm)	$M_{u,theo}$ (kNm)	$M_{u,exp}/M_{u,theo}$	$M_{cr,exp}/M_{cr,theo}$
0G−0FA−0PA	28 days	29.7	16.7	11.7	57.7	62.0	5.2	14.3	2.7	692.8	45.7	59.4	5.41	18.74	3.44	14.58	1.29	1.57
20G−0FA−0PA		32.25	12.8	11.6	57.0	63.4	5.1	14.4	2.8	709.9	43.3	57.0	4.15	18.53	3.63	14.70	1.26	1.14
40G−0FA−0PA		33.55	10.3	12.2	57.9	64.0	5.1	12.3	2.4	591.5	31.9	59.6	3.35	18.81	3.72	14.75	1.28	0.90
0G−20FA−0PA		32.8	16.2	10.2	55.4	63.6	5.5	20.8	3.8	1093.1	36.0	53.7	5.27	18.00	3.67	14.72	1.22	1.44
20G−20FA−0PA		31.34	15.4	9.2	55.8	60.3	6.1	24.3	4.0	1246.2	40.0	48.6	5.01	18.13	3.56	14.66	1.24	1.41
40G−20FA−0PA		30.12	15.3	10.7	59.3	71.7	5.5	19.9	3.6	1137.0	40.6	57.6	4.97	19.27	3.47	14.61	1.32	1.43
0G−0FA−20PA		28.12	17.3	10.5	57.8	65.6	5.7	21.5	3.8	1163.8	57.5	54.6	5.62	18.78	3.33	14.50	1.30	1.69
20G−0FA−20PA		29.35	15.9	9.9	57.6	65.2	6.0	20.8	3.5	1091.8	55.9	51.2	5.17	18.73	3.42	14.57	1.29	1.51
40G−0FA−20PA		30.53	15.6	10.8	56.8	68.5	5.4	15.3	2.8	792.6	43.3	55.3	5.07	18.46	3.50	14.62	1.26	1.45
0G−0FA−0PA	6	36.25	11.8	8.6	54.2	63.3	6.3	14.7	2.3	668.1	21.1	45.5	3.84	17.62	3.90	14.85	1.19	0.98
20G−0FA−0PA	months	37.47	13.2	8.4	55.0	63.4	7.0	16.4	2.3	794.4	23.0	42.7	4.29	17.89	3.99	14.89	1.20	1.08
40G−0FA−0PA		41.53	14.1	8.2	54.4	62.5	6.5	16.1	2.5	740.8	26.3	40.5	4.57	17.67	4.25	15.00	1.18	1.07
0G−20FA−0PA		41.63	15.2	8.2	55.0	61.1	7.1	15.0	2.1	658.5	35.0	44.7	4.92	17.87	4.26	15.01	1.19	1.16
20G−20FA−0PA		36.69	15.4	8.5	55.4	63.6	6.4	17.6	2.7	882.3	29.0	46.9	5.01	18.01	3.93	14.87	1.21	1.27
40G−20FA−0PA		38.84	15.1	9.6	57.7	63.4	6.1	14.6	2.4	686.5	49.2	48.5	4.90	18.74	4.08	14.93	1.26	1.20
0G−0FA−20PA		33.56	14.5	9.0	53.9	66.0	5.7	16.6	2.9	824.1	23.6	48.0	4.71	17.52	3.72	14.75	1.19	1.27
20G−0FA−20PA		38.56	12.8	8.3	52.9	62.8	6.6	15.5	2.4	712.3	24.7	43.8	4.16	17.18	4.06	14.92	1.15	1.02
40G−0FA−20PA		37.32	14.1	9.6	56.3	62.4	6.0	14.6	2.4	666.4	45.0	49.4	4.58	18.31	3.98	14.89	1.23	1.15

compared to OPC mixes, consistent with the reduced early-age strength and slower hydration of pozzolanic binders. However, in all binder groups, including OPC, FA, and PA, stiffness increased with higher GFA content. Beams with 40 % GFA exhibited the highest stiffness values at both 28 days and six months, indicating that GFA contributes positively to stiffness development even at early ages. This improvement can be attributed to several mechanisms. The angular shape and rigidity of GFA enhance internal aggregate interlock, while its impermeable nature reduces moisture ingress, helping to mitigate long-term degradation. The pozzolanic ability of GFA, as discussed before, can cause the improvement at six months [20,24]. Moreover, at six months, the stiffness difference between PA or FA beams and their OPC counterparts narrowed or even reversed, with PA and FA beams showing higher stiffness in many cases. This is attributed to the continued pozzolanic reaction of SCMs, which improves the microstructure and supports long-term stiffness retention [20,24]. Overall, the combined use of GFA with PA or FA enhances flexural stiffness over time. Moreover, PA consistently performs on par with FA, reinforcing its suitability as a sustainable SCM alternative.

3.3.4.4. Displacement ductility. Displacement ductility, calculated as the ratio of mid-span deflection at ultimate load to deflection at first steel yield (Fig. 17(d)), provides a measure of each beam's ability to deform inelastically. Adding GFA did not meaningfully alter ductility; values at 28 days and six months remained comparable across the 0, 20 and 40 % mixes. The six-month beams, however, were slightly less ductile than their 28-day counterparts. This reduction follows the same trend observed in flexural stiffness and may be attributed similarly to the effects of drying shrinkage and temperature variations, which can induce microcracks and accelerate long-term degradation of the beams. These factors can limit strain development and reduce the beam's ability to undergo plastic deformation prior to failure [63].

At 28 days, beams incorporating PA or FA exhibited significantly higher ductility compared to OPC mixes, with values ranging from 2.8 to 4.0 versus 2.4–2.8 in the OPC group. This increase can be attributed to better compaction and reduced thermal cracking. These characteristics collectively delay crack coalescence and preserve bond integrity during inelastic deformation. However, within both the PA and FA series, ductility tends to decrease as GFA content increases to 40 %, though beams with 40 % GFA combined with PA or FA still exhibited higher ductility than their OPC counterparts. This decline can be attributed to reduced internal cohesion and compaction challenges at higher GFA levels, as the angular shape and low water absorption of glass particles lead to reduced slump and stiffer mixes, as observed in Fig. 5(a). Inadequate consolidation in low-slump mixes can lead to entrapped air and poor matrix homogeneity, reducing the beam's capacity for inelastic deformation. It can also weaken the bond between concrete and reinforcement, further limiting post-yield ductility [66]. At the six-month mark, however, both PA and FA beams generally exhibit ductility values similar to those of the OPC beams. This may be due to long-term changes in the microstructure, such as increased stiffness from continued pozzolanic reactions and matrix densification, which can reduce deformation capacity. Additionally, environmental exposure over time may have influenced bond conditions or microcracking similarly across all mixes, thereby minimising the ductility advantage initially observed in the SCM beams.

3.3.4.5. Fractural toughness. The energy absorption of the beams, determined by calculating the area under the load-deflection curves, serves as an indicator of beam toughness, as shown in Fig. 17(e). At 28 days, energy absorption fluctuated with GFA content, showing a modest increase at 20 % GFA before decreasing at 40 %. This pattern may be attributed to the friability of GFA [56] and its influence on matrix cohesion, where moderate additions enhance particle interlock and toughness, but higher levels introduce weaker zones that reduce fracture

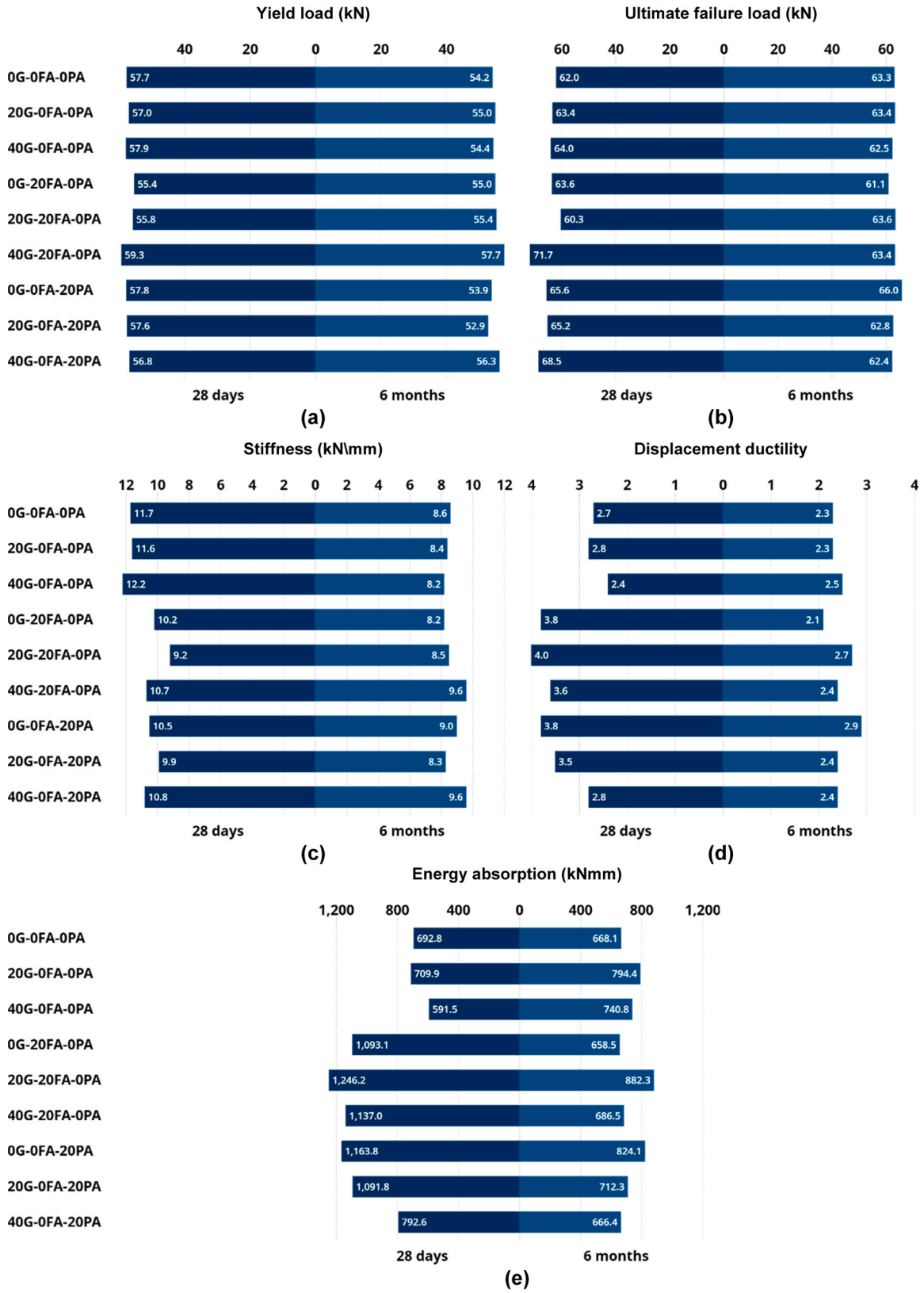

Fig. 17. a) Yield load (kN); (b) Ultimate failure load (kN); (c) Stiffness (kN/mm); (d) Displacement ductility (mm/mm); (e) Energy absorption (kNmm).

energy. However, at six months, the opposite trend is observed, with higher GFA content leading to higher energy absorption. This behaviour is likely attributed to the discussed pozzolanic activity of GFA, which enhances bond strength between the aggregate and the cement matrix over time, requiring more energy to initiate failure.

At 28 days, beams containing PA or FA exhibit significantly higher energy absorption compared to OPC beams across all GFA levels. This improvement is attributed to reduced thermal cracking and improved compaction, which increase bond strength and decrease internal voids, thereby raising the energy required to fracture the concrete. However,

by six months, PA- and FA-modified beams generally performed on par with OPC beams, although individual values fluctuated slightly above or below their OPC counterparts across different GFA levels. This decline may be linked to the same long-term degradation mechanisms that affected flexural stiffness and ductility, such as microcracking, reduced bond performance, and possible early-stage reinforcement deterioration due to environmental exposure. These factors can compromise the energy dissipation capacity of the beams, thereby reducing fracture toughness at later ages [67,68].

3.4. Assessment of serviceability

Ensuring serviceability is as critical as achieving adequate strength in concrete design. Serviceability means the structure continues to perform its intended function under service loads throughout its lifespan. This requires controlling crack widths and limiting deflections. Excessive deflection can be unsightly and uncomfortable, while inadequate crack control may lead to durability issues such as reinforcement corrosion. EC2 was chosen to conduct the assessment due to its comprehensive serviceability and ultimate limit state criteria, suitability for novel materials, and widespread adoption in concrete design [33,69]. EC2 [33] limits the crack width to 0.3 mm and prescribes a maximum deflection of the effective span divided by 250 (5.2 mm for the beams in this study). Fig. 18(a) shows the load corresponding to a 0.3 mm crack width ($P_{0.3Cr}$), determined by DIC analysis, and the load at the maximum allowable deflection ($P_{m.def.}$) derived from load-deflection data via linear interpolation. These results are also presented in Table 4. Higher values of the load corresponding to $P_{0.3Cr}$ and $P_{m.def.}$ indicate a greater capacity to maintain serviceability under higher service loads.

The data reveal that in nearly all beams, $P_{0.3Cr}$ is reached before $P_{m.def.}$, except for PA beams with 0 % and 20 % GFA at 28 days. At 28 days, increasing GFA reduces $P_{0.3Cr}$, indicating diminished serviceability of RC beams. Fig. 18(b) shows the percentage change in $P_{0.3Cr}$ from 28 days to six months. The control beam without GFA shows a 53.8 % reduction over this period. However, at six months, beams with higher GFA levels exhibit an increase in $P_{0.3Cr}$, outperforming the control. These results indicate that although GFA may adversely affect serviceability in the short term, it can enhance long-term performance.

The addition of PA significantly increased $P_{0.3Cr}$ at both 28 days and six months, indicating improved serviceability. At 40 % GFA, PA effectively offset the discussed reduction in $P_{0.3Cr}$ with only GFA at 28 days. At 28 days, PA yielded notably higher $P_{0.3Cr}$ than FA for 0 % and 20 % GFA levels and showed modest improvement at 40 % GFA. At six months, although PA performed slightly below FA across all GFA levels, it still outperformed beams without SCMs. In particular, at 40 % GFA, PA raised $P_{0.3Cr}$ to levels comparable to the 28-day beam with 40 % GFA and PA, and even to the control. Although PA was primarily used as an ASR mitigation SCM, these results demonstrate its effectiveness in enhancing serviceability when combined with GFA in RC beams. Notably, PA helps counteract the negative impact of GFA on serviceability, making it an ideal addition to GFA concrete.

3.5. Experimental vs. theoretical cracking moments and ultimate capacities

This section aims to assess whether EC2-based design equations remain valid for reinforced concrete beams made with non-conventional materials such as GFA, FA, and PA. While the EC2 framework is widely used for conventional concrete, limited research exists on its accuracy and reliability when applied to sustainable concrete mixes with high waste content. This section provides a comparative analysis between experimentally measured and theoretically predicted cracking and ultimate moments. The findings offer practical insights into the conservatism and limitations of existing design models for these novel concretes and suggest where adjustment factors may be warranted for long-term safety or serviceability. The theoretical cracking load ($M_{cr,theo}$) is determined using the design model from EC2 [33] (Eq. 1). The mean tensile strength of concrete (f_{ctm}) is calculated using Eq. 2 from EC2 [33].

$$M_{cr,theo} = \frac{f_{ctm} I_u}{(h - x_u)} \tag{1}$$

$$f_{ctm} = 0.3 f_{ck}^{2/3} \tag{2}$$

$$I_u = \frac{bh^3}{12} + bh\left(\frac{h}{2} - x_u\right)^2 + (\alpha_e - 1)\left[A_s(d - x_u)^2 + A_{s2}(x_u - d_2)^2\right] \tag{3}$$

$$x_u = \frac{\frac{bh^2}{2} + (\alpha_e - 1)[A_s d + A_{s2} d_2]}{bh + (\alpha_e - 1)[A_s + A_{s2}]} \tag{4}$$

f_{ck} is the characteristic compressive strength experimentally determined for each mix as presented in Table 4. Additionally, I_e represents the second moment of area of the uncracked transformed section, x_u is the distance from the neutral axis to the extreme top fibre, and h is the height of the beam. The beam width is denoted by b, while A_s and A_{s2} represent the areas of tensile and compressive reinforcement, respectively. The modular ratio α_e refers to the ratio of the Young's modulus of steel to that of concrete. Fig. 19 shows the ratio of the $M_{cr,theo}$ to the experimental cracking moment ($M_{cr,exp}$), corresponding to the first crack appearance loads discussed in 3.3.1.

At 28 days, the control beam without GFA or SCMs exhibited a cracking moment 57 % higher than predicted. With 20 % GFA, the

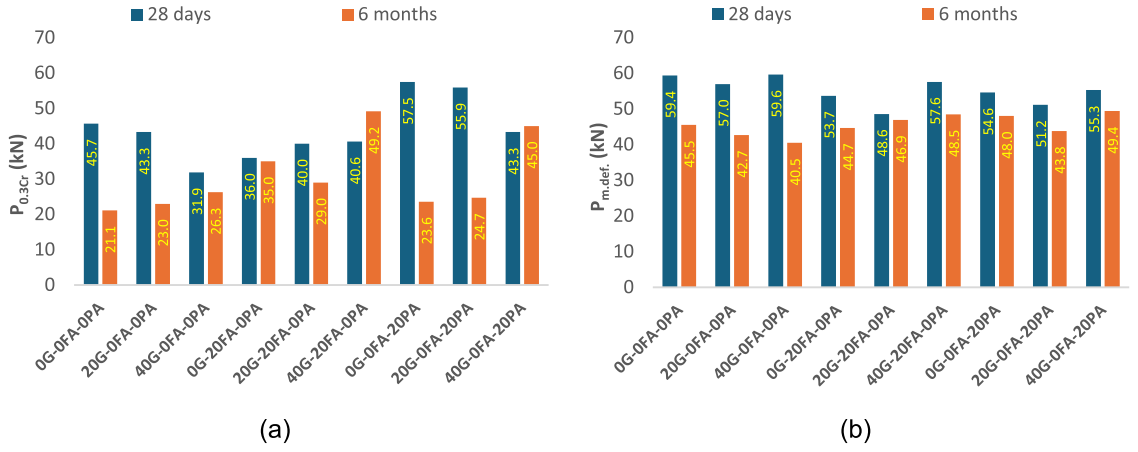

Fig. 18. Load corresponding to: (a) the 0.3 mm crack width ($P_{0.3Cr}$) and (b) maximum permissible deflection ($P_{m.def.}$).

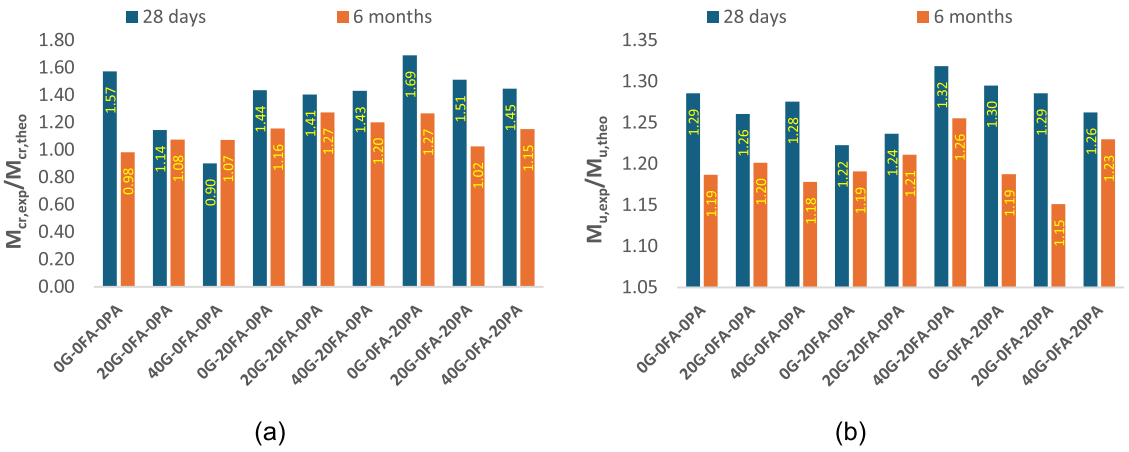

Fig. 19. (a) Experimental vs theoretical cracking moments and (b) Experimental vs theoretical ultimate capacities.

experimental cracking moment was 14 % higher than predicted, whereas at 40 % GFA, it was 10 % lower. These results suggest that the EC2 model [33] is reasonably accurate for lower GFA levels but may require revision for RC beams with higher GFA content to ensure a higher margin of safety. At six months, the experimental values closely matched the predicted ones, suggesting that the design model should be revised to be more conservative in the long term, particularly for GFA concrete without SCM.

At 28 days, the inclusion of FA/PA results in a significant increase over the predicted values, attributable to the factors discussed in 3.3.1. In particular, for beams with 20 % and 40 % GFA, both FA and PA achieved significantly higher safety margins than beams with GFA alone, indicating that the EC2 model [33] is more conservative for beams incorporating GFA and SCMs. At six months, however, FA/PA beams exhibited lower conservative cracking moments with reduced safety margins, without the pronounced increase observed at 28 days. This suggests that while the EC2 model [33] may be viable for ensuring short-term conservatism, additional safety factors may be considered to meet the serviceability limit state for long-term performance.

The theoretical ultimate load, $M_{u,theo}$, is calculated using the simplified rectangular stress block analysis described in EC2 [33]. A_s denotes the area of the tensile reinforcement, f_{yk} and f_{ck} represent the characteristic strengths of the steel rebar and concrete, respectively, and b is the width of the beam. z represents the lever arm, defined as the distance between the tensile and compressive resultants, and a denotes the depth of the equivalent rectangular stress block in the concrete section. The equations were derived using a stress block coefficient of 0.8 and partial safety factors of 1.5 for concrete and 1.15 for steel rebar.

$$M = 0.87 A_s f_{yk} z \tag{5}$$

$$z = d - \frac{a}{2} \tag{6}$$

$$a = 1.63 \frac{A_s f_{yk}}{f_{ck} b} \tag{7}$$

Fig. 19 presents the ratio between $M_{u,theo}$ and the experimental ultimate load, $M_{u,exp}$, which corresponds to the yield loads discussed in 3.3.2. At 28 days, the ultimate capacities show safety margins between 22 % and 32 % for beams with GFA, FA, and PA, confirming the viability of the EC2 model [33] for RC beams with GFA and PA at the ultimate limit state. However, at six months, the safety margins drop to 15 %-26 %, suggesting that additional safety factors may be needed for long-term performance.

4. Conclusions

The following conclusions were drawn based on the results of this study.

- Increasing GFA improved concrete strength. At 28 days, 50 % GFA boosted compressive strength by 16.4 %, rising to 20.4 % at six months, indicating its pozzolanic activity. Only 10 % of PA matched OPC and FA strength at 28 days, while 20 % of PA achieved similar strength as OPC and FA at six months, suggesting PA's potential as a strength-wise FA alternative.
- GFA increased the cracking tendency at 28 days but reduced it by six months. PA significantly decreased crack widths at 28 days compared to OPC and slightly outperformed FA. By six months, PA showed marginally higher crack widths than FA but remained well below the OPC series, demonstrating its effectiveness in GFA concrete beams for serviceability.
- The inclusion of GFA and PA did not significantly affect the yield or ultimate loads of beams at 28 or six months. A slight decrease in yield load at six months was observed across all beams, potentially due to beam degradation over time. Variations in this decrease in yield load suggest that GFA and PA may mitigate beam degradation. GFA acts as an impermeable barrier against external attacks, while PA enhances the microstructure through pozzolanic reactions, creating a denser matrix.
- All beam types showed reduced stiffness at six months compared to 28 days, further suggesting beam degradation. While GFA did not significantly affect stiffness in OPC beams, beams with PA showed improved stiffness at six months as GFA content increased, indicating reduced rebar degradation due to microstructural enhancement. Both PA and FA showed similar effectiveness in enhancing stiffness.
- GFA did not significantly affect displacement ductility. Fracture toughness decreased with higher GFA content at 28 days but improved at six months, indicating stronger bonds due to GFA's pozzolanic activity. Both displacement ductility and energy absorption were enhanced by PA and FA at 28 days, which is attributed to reduced thermal cracking and improved compaction. By six months, the performance of both PA and FA closely aligned with that of OPC beams.
- In the short term, GFA adversely affected serviceability, but its long-term impact was positive. Furthermore, incorporating PA markedly improved serviceability at both stages, demonstrating its value beyond merely mitigating ASR in GFA concrete beams.
- Adjustments to safety factors may be needed for serviceability limit state design in GFA-SCM beams, particularly for crack control, while refinements to ultimate limit state design are recommended to enhance long-term conservatism.

The results of this study strongly support the use of waste glass in structural applications, along with pond ash as an ASR mitigation SCM, with up to 20 % OPC replacement. With pond ash, up to 40 % of waste glass can be utilised in structural beams. This study also contributes to sustainability goals in the construction industry by demonstrating that two waste materials can be effectively used in structural concrete.

Author statement

We, the authors of the manuscript titled "Flexural Behaviour, Cracking, and Serviceability of Sustainable RC Beams with Waste Glass Fine Aggregate and Pond Ash ", declare the following

Author contributions and approval

All authors have made substantial contributions to the work. The contributions are detailed in the CRediT authorship contribution statement included in the manuscript. All authors have reviewed and approved the final version of the manuscript and consent to its submission to the journal.

Originality and exclusivity

This manuscript is original and has not been published or submitted elsewhere. It is not under consideration by any other journal.

Funding

This project is funded by ARC-ITRH (Australian Research Council-Industrial Transformation Research Hub) research grant (IH200100010) allocated for Transformation of Reclaimed Waste Resources to Engineered Materials and Solutions for a Circular Economy (TREMS).

CRediT authorship contribution statement

V. Fernando: Writing – original draft, Investigation, Formal analysis, Data curation, Conceptualization. **R. Bastola:** Writing – review & editing, Investigation, Formal analysis, Data curation. **W. Lokuge:** Writing – review & editing, Validation, Supervision, Resources, Project administration, Methodology, Conceptualization, Funding acquisition. **C. Gunasekara:** Writing – review & editing, Validation, Supervision, Methodology, Conceptualization. **H. Wang:** Writing – review & editing, Validation, Supervision, Methodology, Conceptualization, Funding acquisition.

Declaration of Competing Interest

The authors declare the following financial interests/personal relationships which may be considered as potential competing interests: Weena Priyanganie Lokuge reports was provided by Australian Research Council (Industrial Transformation Research Hub - research grant IH200100010). Hao Wang reports was provided by Australian Research Council (Industrial Transformation Research Hub - research grant IH200100010). If there are other authors, they declare that they have no known competing financial interests or personal relationships that could have appeared to influence the work reported in this paper.

Acknowledgements

This project is funded by ARC-ITRH (Australian Research Council-Industrial Transformation Research Hub) research grant (IH200100010) allocated for Transformation of Reclaimed Waste Resources to Engineered Materials and Solutions for a Circular Economy (TREMS). The first author gratefully acknowledged the financial assistance provided by the UniSQ international stipend research scholarship (through TREMS) and the UniSQ international fees research scholarship.

Data availability

Data will be made available on request.

References

[1] Schneider M, Romer M, Tschudin M, Bolio H. Sustainable cement production—present and future. Cem Concr Res 2011;41:642–50. https://doi.org/10.1016/J.CEMCONRES.2011.03.019.
[2] Gallagher L., Peduzzi P. Sand and Sustainability: Finding New Solutions for Environmental Governance of Global Sand Resources. Geneva: 2019.
[3] Ahmed KS, Rana LR. Fresh and hardened properties of concrete containing recycled waste glass: a review. J Build Eng 2023;70. https://doi.org/10.1016/j.jobe.2023.106327.
[4] Saha A, Aditto FS, Kundu L, Sobuz MHR, Sunny MMH. Analysis of waste glass as a partial substitute for coarse aggregate in self-compacting concrete: an experimental and machine learning study. J Build Eng 2024;98. https://doi.org/10.1016/j.jobe.2024.111112.
[5] Nature. Glass is the hidden gem in a carbon-neutral future. vol. 599. 2021. https://doi.org/10.1038/d41586-021-02992-8.
[6] Topçu IB, Canbaz M. Properties of concrete containing waste glass. Cem Concr Res 2004;34:267–74. https://doi.org/10.1016/J.CEMCONRES.2003.07.003.
[7] Olofinnade OM, Ndambuki JM, Ede AN, Booth C. Application of waste glass powder as a partial cement substitute towards more sustainable concrete production. Int J Eng Res Afr 2017;31:77–93. https://doi.org/10.4028/www.scientific.net/JERA.31.77.
[8] Disfani MM, Arulrajah A, Bo MW, Sivakugan N. Environmental risks of using recycled crushed glass in road applications. J Clean Prod 2012;20:170–9. https://doi.org/10.1016/J.JCLEPRO.2011.07.020.
[9] De Castro S, De Brito J. Evaluation of the durability of concrete made with crushed glass aggregates. J Clean Prod 2013;41:7–14. https://doi.org/10.1016/j.jclepro.2012.09.021.
[10] Batayneh M, Marie I, Asi I. Use of selected waste materials in concrete mixes. Waste Manag 2007;27:1870–6. https://doi.org/10.1016/j.wasman.2006.07.026.
[11] Taha B, Nounu G. Utilizing waste recycled glass as Sand/Cement replacement in concrete. J Mater Civ Eng 2009;21:709–21. https://doi.org/10.1061/(ASCE)0899-1561(2009)21:12(709).
[12] Rajabipour F, Giannini E, Dunant C, Ideker JH, Thomas MDA. Alkali–silica reaction: current understanding of the reaction mechanisms and the knowledge gaps (https://doi.org/) Cem Concr Res 2015;76:130–46. https://doi.org/10.1016/j.cemconres.2015.05.024.
[13] Maraghechi H, Shafaatian SMH, Fischer G, Rajabipour F. The role of residual cracks on alkali silica reactivity of recycled glass aggregates. Cem Concr Compos 2012;34:41–7. https://doi.org/10.1016/j.cemconcomp.2011.07.004.
[14] Abdallah S, Fan M. Characteristics of concrete with waste glass as fine aggregate replacement. Int J Eng Tech Res (IJETR) 2014;2:11–7.
[15] Ismail ZZ, AL-Hashmi EA. Recycling of waste glass as a partial replacement for fine aggregate in concrete. Waste Manag 2009;29:655–9. https://doi.org/10.1016/j.wasman.2008.08.012.
[16] Du H, Tan KH. Use of waste glass as sand in mortar: part II - Alkali-silica reaction and mitigation methods. Cem Concr Compos 2013;35:118–26. https://doi.org/10.1016/j.cemconcomp.2012.08.029.
[17] Shafaatian SMH, Akhavan A, Maraghechi H, Rajabipour F. How does Fly ash mitigate alkali–silica reaction (ASR) in accelerated mortar bar test (ASTM C1567)? (https://doi.org/) Cem Concr Compos 2013;37:143–53. https://doi.org/10.1016/j.cemconcomp.2012.11.004.
[18] Pereira De Oliveira LA, Castro-Gomes JP, Santos P. Mechanical and durability properties of concrete with ground waste glass sand. 11 DBMC Int Conf Durab Build Mater Compon 2008.
[19] Topçu IB, Boğa AR, Bilir T. Alkali-silica reactions of mortars produced by using waste glass as fine aggregate and admixtures such as Fly ash and Li2CO3. Waste Manag 2008;28:878–84. https://doi.org/10.1016/j.wasman.2007.04.005.
[20] Fernando V, Lokuge W, Seligmann H, Wang H, Gunasekara C. Sustainable mortar with waste glass and Fly ash: impact of glass aggregate size and Life-Cycle assessment (https://doi.org/) Recycling 2025;10. https://doi.org/10.3390/recycling10040133.
[21] Yimam YA, Warati GK, Fantu T, Paramasivam V, Selvaraj SK. Effect of pond ash on properties of C-25 concrete. Mater Today Proc 2021;46:8296–302. https://doi.org/10.1016/j.matpr.2021.03.258.
[22] Harris DJ, Heidrich C, Feuerborn J. Glob Asp coal Combust Prod 2019.
[23] Ash Development Association of Australia. Annual Production and Utilisation Survey Report. 2023.
[24] Fernando WCV, Lokuge W, Wang H, Gunasekara C, Dhasindrakrishna K. Sustainable mortar with waste glass fine aggregates and pond ash as an alkali-silica reaction suppressor (https://doi.org/) Case Stud Constr Mater 2025;22. https://doi.org/10.1016/j.cscm.2025.e04269.
[25] Mustafa TS, El. Beshlawy SA, Nassem AR. Experimental study on the behavior of RC beams containing recycled glass. Constr Build Mater 2022;344:128250. https://doi.org/10.1016/j.conbuildmat.2022.128250.
[26] ASTM International. ASTM C566 - Standard Test Method for Total Evaporable Moisture Content of Aggregate by Drying. Annual Book of ASTM Standards 2023.

[27] ASTM International. ASTM C128 - Standard Test Method for Relative Gravity (Specific Gravity) and Absorption of Fine Aggregate. Annual Book of ASTM Standards 2022.
[28] ASTM International. ASTM C33/ C33M - Standard Specification for Concrete Aggregates. Annual Book of ASTM Standards 2023.
[29] Standards Australia. AS 1012.3.1 Methods of Testing Concrete - Determination of properties related to the consistency of concrete - Slump test. Sydney: 2014.
[30] Standards Australia. AS 1012.9 - Methods of testing - Compressive strength tests - Concrete, mortar and grout specimens. Sydney: 2014.
[31] Standards Australia. AS 1012.10 - Methods of testing - Determination of indirect tensile strength of concrete cylinders ('Brazil' or splitting test). Sydney: 2000.
[32] Standards Australia. AS 1012.11 - Methods of testing - Determination of the modulus of rupture. Sydney: 2000.
[33] BS EN 1992-1-1. Eurocode 2: Design of concrete structures - Part 1-1: General rules and rules for buildings. British Standards Institution 2004. https://doi.org/ [Authority: The European Union Per Regulation 305/2011, Directive 98/34/EC, Directive 2004/18/EC].
[34] Al-Abdwais AH, Al-Mahaidi RS. Experimental and finite element analysis of flexural performance of RC beams retrofitted using near-surface mounted with CFRP composites and cement adhesive. Eng Struct 2021;241:112429. https://doi.org/10.1016/j.engstruct.2021.112429.
[35] Abu Maraq MA, Tayeh BA, Ziara MM, Alyousef R. Flexural behavior of RC beams strengthened with steel wire mesh and self-compacting concrete jacketing - experimental investigation and test results. J Mater Res Technol 2021;10:1002–19. https://doi.org/10.1016/j.jmrt.2020.12.069.
[36] Jin L, Zhang J, Song B, Li D, Li P, Du X. Effect of stirrups on shear performance of geometrically-similar reinforced concrete deep beams: an experimental study. Eng Struct 2023;295:116883. https://doi.org/10.1016/j.engstruct.2023.116883.
[37] Adaway M, Wang Y. Recycled glass as a partial replacement for fine aggregate in structural concrete -Effects on compressive strength. Electron J Struct Eng 2015;14:116–22.
[38] Su Q, Xu J. Compression behavior and permeability of concrete composed of glass sand and rice husk ash. J Build Eng 2023;76. https://doi.org/10.1016/j.jobe.2023.107095.
[39] Bisht K, Ramana PV. Experimental investigation of strength, drying shrinkage, freeze and thaw and fire attack properties of concrete mixes with beverage glass waste as fine aggregate. Structures 2022;36:358–71. https://doi.org/10.1016/j.istruc.2021.12.019.
[40] Surendran H, Akhas PK. Properties of high-performance concrete incorporating toughened glass waste coarse aggregate: an experimental study. Structures 2024;60:105897. https://doi.org/10.1016/j.istruc.2024.105897.
[41] Kurda R, de Brito J, Silvestre JD. Influence of recycled aggregates and high contents of Fly ash on concrete fresh properties. Cem Concr Compos 2017;84:198–213. https://doi.org/10.1016/j.cemconcomp.2017.09.009.
[42] Nayak DK, Abhilash PP, Singh R, Kumar R, Kumar V. Fly ash for sustainable construction: a review of Fly ash concrete and its beneficial use case studies. Clean Mater 2022;6:100143. https://doi.org/10.1016/j.clema.2022.100143.
[43] Jamellodin Z, Qian Yi L, Latif QBAI, Algaifi HA, Hamdan R, Al-Gheethi A. Evaluation of fresh and hardened concrete properties incorporating glass waste as partial replacement of fine aggregate. Sustain (Switz) 2022;14. https://doi.org/10.3390/su142315895.
[44] Gorospe K, Booya E, Ghaednia H, Das S. Strength, durability, and thermal properties of glass aggregate mortars. J Mater Civ Eng 2019;31. https://doi.org/10.1061/(ASCE)MT.1943-5533.0002884.
[45] Rajabipour F, Maraghechi H, Fischer G. Investigating the Alkali-Silica reaction of recycled glass aggregates in concrete materials. J Mater Civ Eng 2010;22:1201–8. https://doi.org/10.1061/(asce)mt.1943-5533.0000126.
[46] Steyn ZC, Babafemi AJ, Fataar H, Combrinck R. Concrete containing waste recycled glass, plastic and rubber as sand replacement. Constr Build Mater 2021;269:121242. https://doi.org/10.1016/j.conbuildmat.2020.121242.
[47] Hong S-Y, Glasser FP. Alkali sorption by C-S-H and C-A-S-H gels: part II. Role of alumina (https://doi.org/) Cem Concr Res 2002;32:1101–11. https://doi.org/10.1016/S0008-8846(02)00753-6.
[48] Qin J, Geng Y, Chang YC, Zhang H, Wang YY. Probabilistic model for compressive strength of recycled aggregate concrete accounting for uncertainty of recycled aggregates from different sources. Constr Build Mater 2025;479:141485. https://doi.org/10.1016/j.conbuildmat.2025.141485.
[49] Zong S, Chang C, Rem P, Gebremariam AT, Di Maio F, Lu Y. Research on the influence of particle size distribution of high-quality recycled coarse aggregates on the mechanical properties of recycled concrete. Constr Build Mater 2025;465:140253. https://doi.org/10.1016/j.conbuildmat.2025.140253.
[50] Borhan TM. Properties of glass concrete reinforced with short basalt fibre. Mater Des 2012;42:265–71. https://doi.org/10.1016/j.matdes.2012.05.062.
[51] Limbachiya MC. Bulk engineering and durability properties of washed glass sand concrete. Constr Build Mater 2009;23:1078–83. https://doi.org/10.1016/j.conbuildmat.2008.05.022.
[52] Taha B, Nounu G. Properties of concrete contains mixed colour waste recycled glass as sand and cement replacement. Constr Build Mater 2008;22:713–20. https://doi.org/10.1016/j.conbuildmat.2007.01.019.
[53] Sharifi Y, Houshiar M, Aghebati B. Recycled glass replacement as fine aggregate in self-compacting concrete. Front Struct Civ Eng 2013;7:419–28. https://doi.org/10.1007/s11709-013-0224-8.
[54] Moghaddam F, Sirivivatnanon V, Vessalas K. The effect of Fly ash fineness on heat of hydration, microstructure, flow and compressive strength of blended cement pastes. Case Stud Constr Mater 2019;10. https://doi.org/10.1016/j.cscm.2019.e00218.
[55] Sarkar R, Singh N, Das SK. Effect of addition of pond ash and Fly ash on properties of ash-clay burnt bricks. Waste Manag Res 2007;25:566–71. https://doi.org/10.1177/0734242×07080114.
[56] Polley C, Cramer SM, Cruz RV. De la. Potential for using waste glass in portland cement concrete. J Mater Civ Eng 1998;10:210–9. https://doi.org/10.1061/(asce)0899-1561(1998)10:4(210).
[57] Wei L, Zhang N, Sun L. Rebar corrosion and bond in concrete with recycled glass granules. J Build Eng 2024;98. https://doi.org/10.1016/j.jobe.2024.111269.
[58] Mardani-Aghabaglou A, Tuyan M, Ramyar K. Mechanical and durability performance of concrete incorporating fine recycled concrete and glass aggregates. Mater Struct/Mater Et Constr 2015;48:2629–40. https://doi.org/10.1617/s11527-014-0342-3.
[59] Wright JR, Cartwright C, Fura D, Rajabipour F. Fresh and hardened properties of concrete incorporating recycled glass as 100% sand replacement. J Mater Civ Eng 2014;26. https://doi.org/10.1061/(ASCE)MT.1943-5533.0000979.
[60] Sun Z, Fu L, Feng DC, Vatuloka AR, Wei Y, Wu G. Experimental study on the flexural behavior of concrete beams reinforced with bundled hybrid steel/FRP bars. Eng Struct 2019;197:109443. https://doi.org/10.1016/j.engstruct.2019.109443.
[61] Saha AK. Effect of class f Fly ash on the durability properties of concrete. Sustain Environ Res 2018;28:25–31. https://doi.org/10.1016/j.serj.2017.09.001.
[62] Zhao XM, Wu YF, Leung AYT. Analyses of plastic hinge regions in reinforced concrete beams under monotonic loading. Eng Struct 2012;34:466–82. https://doi.org/10.1016/j.engstruct.2011.10.016.
[63] ACI Committee 224. ACI 224R-01 - Control of Cracking in Concrete Structures. Farmington Hills, MI, USA: 2001.
[64] Ma Z, Zhu F, Ba G. Effects of freeze-thaw damage on the bond behavior of concrete and enhancing measures. Constr Build Mater 2019;196:375–85. https://doi.org/10.1016/j.conbuildmat.2018.11.041.
[65] Wang ZH, Li L, Zhang YX, Wang WT. Bond-slip model considering freeze-thaw damage effect of concrete and its application. Eng Struct 2019;201:109831. https://doi.org/10.1016/j.engstruct.2019.109831.
[66] ACI Committee 309. ACI 309R-05 - Guide for Consolidation of Concrete. Farmington Hills, MI, USA: 2005.
[67] Khalilpour S, BaniAsad E, Dehestani M. A review on concrete fracture energy and effective parameters. Cem Concr Res 2019;120:294–321. https://doi.org/10.1016/j.cemconres.2019.03.013.
[68] Won JP, Park CG. Effect of environmental exposure on the mechanical and bonding properties of hybrid FRP reinforcing bars for concrete structures. J Compos Mater 2006;40:1063–76. https://doi.org/10.1177/0021998305057362.
[69] Ismail MK, Hassan AAA, AbdelAleem BH, El-Dakhakhni W. Flexural behavior and cracking of lightweight RC beams containing coarse and fine slag aggregates. Structures 2023;47:1005–19. https://doi.org/10.1016/j.istruc.2022.11.065.